2007-11-30

Scandium Oxide Thin Films and Their Optical Properties in the Extreme Ultraviolet

Guillermo Antonio Acosta
Brigham Young University - Provo

SCANDIUM OXIDE THIN FILMS AND THEIR OPTICAL PROPERTIES IN THE EXTREME ULTRAVIOLET

by

Guillermo Acosta

A dissertation submitted to the faculty of
Brigham Young University
in partial fulfillment of the requirements for the degree of

Doctor of Philosophy

Department of Physics and Astronomy
Brigham Young University
December 2007

BRIGHAM YOUNG UNIVERSITY

GRADUATE COMMITTEE APPROVAL

of a dissertation submitted by

Guillermo Acosta

This dissertation has been read by each member of the following graduate committee and by a majority vote has been found to be satisfactory.

Date	David D. Allred, Chair
Date	R. Steven Turley
Date	Lawrence B. Rees
Date	Richard Vanfleet
Date	Branton Campbell

BRIGHAM YOUNG UNIVERSITY

As chair of the candidate's graduate committee, I have read the dissertation of Guillermo Acosta in its final form and have found that (1) its format, citations, and bibliographical style are consistent and acceptable and fulfill university and department style requirements; (2) its illustrative materials including figures, tables, and charts are in place; and (3) the final manuscipt is satisfactory to the graduate committee and is ready for submission to the university library.

Date

David D. Allred
Chair, Graduate Committee

Accepted for the Department

J. Ward Moody
Graduate Coordinator

Accepted for the College

Thomas W. Sederberg
Associate Dean, The College of Physical and Mathematical Sciences

ABSTRACT

SCANDIUM OXIDE THIN FILMS AND THEIR OPTICAL PROPERTIES
IN THE EXTREME ULTRAVIOLET

Guillermo Acosta

Department of Physics and Astronomy

Doctor of Philosophy

This study reports on the physical and optical characterization of scandium oxide thin films. Thin films of scandium oxide, 20-40 nm thick, were deposited on silicon wafers, quartz slides, and silicon photodiodes by reactively sputtering scandium in an oxygen environment. These samples were characterized using ellipsometry, high-resolution transmission electron microscopy, scanning transmission electron microscopy, and energy dispersive x-ray analysis. A 28.46 nm thick scandium oxide thin film was measured in the Extreme Ultraviolet (EUV) from 2.7 to 50 nm (459.3 to 24.8 eV) using synchrotron radiation at the Advanced Light Source Beamline 6.3.2 at the Lawrence Berkeley National Laboratory. In these measurements, a new method for data collection was used, in which the reflection and transmission data were collected simultaneously. Analysis of the EUV reflection and transmission data was performed using a front-side reflection, matrix-multiplication technique, which is novel among EUV analytical practice. During data analysis, a new weighting scheme was used, named "adaptive weighting". This analysis provides the first experimentally determined optical constants n and k for scandium oxide thin films from 4.5-30 nm. Also, the

positions of the L_2 and L_3 electronic transitions of scandium oxide have been measured, at 3.069 and 3.101 nm (404.0 and 399.9 eV), respectively, while the measurements near the M transition suggest it to be at approximately 31.5 nm (39.4 eV). Comparing the electronic transition positions of scandium oxide to those of scandium show that the oxidation of scandium shifts the positions to lower energies. For L_2 the shift is about 1.8 eV, for L_3 the shift is about 1.4 eV, and for M the shift is about 1.9 eV. The binding energies of scandium oxide are greater than those of scandium, as is expected for an oxide compared to its parent metal. This trend in the shift of the transition positions is unexpected, and warrants further investigation.

ACKNOWLEDGMENTS

Only with the selfless contributions from many dear friends and colleagues has this project been able to come to completion. I owe a great debt to the Physics Department staff, especially Mr. Wes Lifferth, Mr. Mark Erickson, Mrs. Nan Ellen Ah You, Mr. Scott Daniel, Mr. John Ellsworth, Mr. Freeman Anderson, and Mr. Joe Young, as well as a number of student workers who have helped me in the front office, labs, and shops through the years. Also, I am thankful for the assistance and encouragement I have recieved from fellow students, in the classroom and in the lab: Guillermo Herrera, Dan Ludwigsen, Matt Squires, David Balough, Xi Chen, Jed Whitaker, Chad Junkermier, Jed Johnson, Niki Farnsworth-Brimhall, Stephanie Magleby, Jared Daley, and Jared Stenson. Data collection at the Advanced Light Source at Lawrence Berkeley National Laboratory would not have been possible without the tremendous generosity of Andy Aquila, Dr. Erik Gullikson, and many of the staff members in the labs and in the offices. I offer a very special thanks to Dr. Richard Vanfleet, whose selfless contriubutions of time, energy, and insight made the sample characterization with electron microscopy in these experiments a success. In hindsight I can say that this characterization is so valuable that I cannot imagine this project yeilding results half as nice without it. I am very appreciative of the support I have recieved from the Western Alliance to Expand Student Opportunities through the Minority Graduate Education @ Mountain States Alliance, the NASA Space Grant Consortium, the Society of Photographic Instrumentation Engineers, the Society of Vacuum Coaters, and the Society for Advancement of Chicanos and Native Americans in the Sciences. And, of course, I am very fortunate for the instruction and guidance I have had from my professors, most especially Dr. David Allred, Dr. Larry Knight, Dr. Robert Davis, Dr. Larry Rees, Dr. Eric Hirschmann, and Dr. Steven Turley. Everyone, thank you.

Contents

List of Tables

List of Figures

1 The Extreme Ultraviolet and Thin Films

Unlike the visible part of the electromagnetic spectrum, the Extreme Ultraviolet (EUV) is a loosely defined region of light, with a wavelength range in the neighborhood of 5-40 nm. The EUV is bordered at the short wavelength end by the soft x-rays, beyond which lie x-rays and gamma rays. At the long wavelength end, the EUV bleeds into the vacuum ultraviolet, followed by the ultraviolet and visible spectra. Coincidentally, this energy regime also hosts two peculiarities which foster intriguing challenges for the materials scientist:

- The energies they carry are comparable to the binding energies atoms have for their core electrons, and
- The wavelengths of EUV photons approach atomic dimensions.

Photons with energy close to that necessary for exciting an electron from its orbital lead to a resonance at that energy. Optically, the ramifications of this manifest themselves in the complex index of refraction, $N = n - ik$, which has a strong frequency dependence. The real part of N, called the refractive index n, exhibits this dependence particularly acutely. Resonances also occur in other parts of the electromagnetic spectrum (such as between the infrared and the visible, and between the visible and the ultraviolet). Optically, though, the EUV is additionally complicated by the characteristically short wavelengths being on the same scale of not only atomic dimensions, but also physical and structural features present in materials. The nanoscale attributes, or imperfections, of a coating are of little consequence when considering optical performance in other ranges of light. In the EUV, however, their presence can weigh in significantly in the total performance of a coating.[1]

Overall, the EUV can be summarized as a region where most materials exhibit large absorption. Coupled with the reality of the lack of availability of sources for high-intensity EUV light, experiments to study the optical properties of materials in the EUV are more challenging still. In general, the bulk reflectivities of most materials at normal incidence in the EUV are less than 7%. With the strong absorption and low reflectivity, experiments for studying materials in this region are best done using thin films.[1]

Thin films, too, are only loosely defined. A thin film is literally any material that is thin, with a substantial surface area compared to its volume. Foils can be considered thin films, as are coatings

on surfaces (such as silver on glass to form mirrors, and chrome on steel bumpers). Among material scientists, thin films generally have thicknesses between 10 microns and 50 nm, with the distinction being made in recent years for films thinner than 50 nm as ultrathin films.[2]

Regarding use in the EUV, studying a material as a thin film is advantageous because, even though the high degree of absorption still exists, the sample of the material has very little "depth" with which to absorb light. In principle then, thin films can be used for making transmission measurements that are not possible when considering bulk materials in the EUV. Using thin films assists in resolving the issue of high absorption in the EUV, and also in addressing the problem of characteristically low reflectance. This is done by taking advantage of constructive interference among light reflecting from two or more material interfaces to achieve higher reflectivities than a bulk material would have. Here, too, it is possible to make reflection measurements of a material using thin films that would otherwise be unavailable.[3]

It is important to acknowledge that the optical properties of the thin films will resemble those of the bulk material, but not match exactly. Optical constants acceptable for describing the performance of a bulk material in the EUV are most likely inappropriate in describing a thin film.[3] In fact, from the definition of a thin film having a substantial surface area compared to its volume, it can be seen that bulk materials and thin films need to be considered differently. When contemplating a bulk material, it can be imagined that from within the volume, at the nanoscale, the material appears the same in all directions. From within the volume of a thin film, however, the surface (or at least the effects of the surface) will be "noticeable" in one direction, possibly two. Atoms near the surface will experience a distinctly different local environment than atoms deeper in the volume, especially in comparison to those deep within the volume of a bulk material. Issues such as surface specific atomic placement, different bonding structures among atoms (and possibly between atoms of different materials), and mobility can potentially influence the behavior of atoms near the surface. This requires that optical constants specific to a thin film of a material, even specific to the method of deposition, be verified or determined before critical calculations are made.

Despite having energies beyond those detectable by the human eye, optics and optical coatings in the EUV is lively field of research. Most prominently, high-energy optics has an application in EUV lithography, the dominant method by which microelectronics are manufactured today. Highly reflective coatings used on lithographic optics enhances the efficiency of the method. Continued development of highly reflective coatings at shorter wavelengths will allow for patterning to be performed with shorter wavelengths still, which would lead to even smaller feature sizes, in turn

leading to smaller transistors. In the scientific arena, the EUV region contains the signatures of astronomical phenomena, as well as the "water window", which is important to biologists as it is the small region of light where proteins are absorbing, and cytoplasm is transparent. Research in a variety of fields which use EUV lasers also benefits from the study of optical properties of promising materials. In this regard, the types of coatings of interest are not limited to those highly reflective in nature, but also includes coatings with narrow transmission bands, wide transmission bands with steep edges, and low and high pass filters.[3, 4]

2 Scandium

Scandium is a rare earth metal, and is the first of the transition metals on the periodic chart. Though the rare earths are usually acknowledged as the group of elements with atomic numbers 57-71, scandium, atomic number 21, and yttrium, atomic number 39, have properties similar to those of the rare earths, and are often found in nature with the rare earth elements. Since the rare earth industry developed in the early 1800's, little significant technological use has been found for scandium.[5] Recently, scandium has been used for high-strength, lightweight material applications in the aircraft industry, and in aluminum alloys to control grain size during welding processes. However, titanium performs adequately for these types of applications, and is far more plentiful (and thereby less expensive) than scandium.[6]

With three free electrons in its valence shell, scandium readily bonds with neighboring elements. The only known mineral with as significant concentration of scandium is thortveitite, in which scandium mostly exists as scandium silicide. Upon exposure to the oxygen in air, pure scandium immediately begins to form scandium oxide, Sc_2O_3. Another source of scandium is the solvent extraction process used in the recovery of uranium from its ores. Here the scandium content is low, but after accumulating in the organic solvent used worthwhile amounts of scandium can be harvested.[5, 6]

2.1 The Theoretical Promise of Scandium for Highly Reflective Multilayer Mirrors in the EUV

In 1998, the Russian research team led by Uspenskii published "Highly reflective multilayer mirrors for a vacuum-ultraviolet interval of 35-50 nm". This paper was a landmark in terms of current research involving scandium, since very few publications existed that dealt with studying the material in any capacity.[7, 8] Uspenskii theorized a reflectivity of 67-72 % with light having 49.2-38.5 nm wavelengths.[9] These predicted values totally eclipsed previous calculations using Os/Si, Ir/Si, Os/Al, and Ir/Al multilayer coatings to achieve 30-35% reflectance in this spectral region. In this wavelength range, there is a need for the development of highly reflective coatings, as it is between the areas where Al or LiF reflectors are effective (wavelengths greater than 100 nm) and the region where Mo/Si multilayer coatings are used (from 13-30 nm). Applications such as X-ray lasers, astrophysics, and microanalysis would benefit from the development of coatings of this sort. Experimental results

included in the paper showed impressive reflectivity measurements of several multilayer coatings at specific wavelengths. Still, all measurements were considerably lower than the theorized values, with reflectivities of 36-54%.[9] For perspective, the highest normal incidence reflectivities of bulk materials at 50 nm are 20-25%, and 5-8% at 35 nm, while the greatest measured reflectivity of a multilayer coating in the EUV, was 20% with 38 nm light, using a Os/Si scheme.

In the multilayer coatings Uspenskii studied, thin films of scandium were used with thin films of silicon. It was acknowledged in the paper that the interface between the two materials was not distinct, with the formation of a scandium silicide compound, Sc_3Si_5, at the juncture. The presence of this scandium silicide was not isolated to just the immediate interface region, but instead appeared to consume the scandium thin film nearly entirely. Electron microscopy of a cross section of one of the multilayer coatings illustrated this. In the images included in the paper, the region that was identified as grains of pure scandium had been reduced from a film between two silicon layers to instead being single clusters of grains suspended in scandium silicide.[9] This would introduce complications to modeling the reflectivity of the coatings. Foremost, properly describing the Sc/Si multilayer would require optical constants for scandium silicide. Also, the miscibility of scandium with its neighboring material would also introduce issues with interfacial roughness and layer uniformity. Each of these complications diminish the reflectivity of the coating.

With these imperfections present in samples Uspenskii studied, the opportunity for further study was noticed by the EUV research community. Despite the large differences between the measured and calculated reflectivities, this preliminary work was still very valuable since it presented scandium as a material with promise for use in highly reflective coatings.

2.2 Experimental Studies of Scandium in the EUV

Following the publication of the 1998 Uspenskii paper, a large amount of experimental work with scandium thin films and their optical properties in the EUV took place. By selecting and summarizing some of the papers published, a synopsis of the experimental work is presented here.

Seely, of the Naval Research Laboratory, collaborated with Uspenskii et al. for further study of the Sc/Si multilayer coating. In 2002, they published the results of using this multilayer material combination to coat a 3600 line/mm grating. At 38 nm and 6 degrees from normal, the coated grating measured an efficiency of 7.2%, which is a factor of 3 greater than the efficiency of the grating when it is coated with gold, which was standard use. Prior to checking the reflectance of

the coated grating, the researchers performed a preliminary experiment to check how well suited optical constants from the standard source, *Handbook of Optical Constants of Solids* by Palik, were for describing the optical properties of the scandium thin films. A Sc/W/Si/W multilayer coating was fabricated and measured at 5 degrees from normal. The tungsten between scandium and silicon was to prevent interdiffusion of materials at the interface. Calculations using Palik optical constants were made to model the reflectance, but the difference between the numerical prediction and the measurement was substantial. Seely et al. instead fabricated a series of scandium and silicon bilayers deposited on photodiodes, each with identical silicon thicknesses and varying scandium thicknesses. Measurements of these samples were used to generate optical constants for scandium in the EUV from 18-68 nm. The measured reflectance of the Sc/W/Si/W multilayer was modeled again, this time using the experimentally determined optical constants, with much better results.[10]

In 2003, the Swedish group led by Eriksson published a paper which studied Cr/Sc multilayer mirrors at considerably shorter wavelengths. Among the shorter wavelengths of the EUV, the "water window" exists between 2.4 and 4.4 nm, which is between the K-edge of carbon (4.99 nm) and the K-edge of oxygen (2.28 nm). This spectral range is of interest to researchers in biological fields as it is an area where the water in the cytoplasm of a cell is transparent, while proteins absorb EUV light of these wavelengths. Other prospects for optical developments in these higher energies include applications in deep-space telescopy, free-electron x-ray lasers, wavelength dispersive detection of light-element x-ray emission, and soft x-ray polarimetry.[11, 12, 13, 14] In this new spectral region, measurements of the Cr/Sc multilayer showed notably good performance (at 3.11 nm, up to 14.5% reflectivity), but fell shy of a calculated reflectivity of 25.6%. Eriksson et al. conjectured that the deficiency in the measured reflectance was likely due to interdiffusion between the chromium and scandium, in addition to a small drift in the periodicity of the multilayer spacing. At these short wavelengths, the consistency of the multilayer spacings are critical since the optimal reflectivity occurs at the absorption edge of one of the materials of the stack, and also since this maximal reflectivity would have a narrow bandwidth.[15]

Uspenskii and Seely published another paper reporting measurements of scandium thin films in the EUV from 17.7-68.8 nm in 2004. As Seely had before, several photodiodes were coated with a Sc/Si bilayer. The thin film of silicon was to act as a protective coating to ensure the scandium thin film did not oxidize or otherwise change. Additionally, this thin film of silicon was to be identical on all of the coated diodes. Uspenskii outlined an approach that capitalized on this identical protection layer and the fact that the scandium thin films were deposited directly onto photodiodes to determine

the optical constants n and k. Part of this approach relied on having several scandium coated diodes with a range of film thicknesses on them, each identically protected. With the data from the coated diodes, ratios could be judiciously taken among them to provide data optimized for a certain wavelength range. It was concluded that the combination of using identically protected thin films deposited on photodiodes and the analytic approach was the solution to eliminating problems with reactive (getter) materials and their potential contamination from exposure to air.[16]

Also in 2004, Spanish researchers, Larruquert et al., reported measurements of scandium thin films made *in-situ*, over the wavelength range 53.6-174.4 nm. In the opening paragraphs, Larruquert was clear about the need to measure truly pure scandium thin films, noting that it was likely that much of the earlier work reported by other researchers was done with tainted scandium films that had been exposed to air and possibly solvents as well. Additional measurements of the films made *ex-situ* extended the wavelength range to cover 6.7-174.4 nm. The thin films studied in the *in-situ* experiments were scandium thin films deposited onto grids with a supportive carbon film. For the subsequent *ex-situ* studies, the samples were coated with another carbon film, so that the scandium thin film was protected above and below by carbon. These studies of scandium thin films provided experimentally determined optical constants from 6.7-30 nm and from 42-174.4 nm, while the optical constants for the 30-42 nm gap were calculated.[17]

Lastly, Aquila at Lawrence Berkeley National Laboratory completed an exhaustive experimental measure of scandium's optical properties over the 0.95-24.8 nm wavelength range, with particular attention paid to the region surrounding the scandium edge near 3.1 nm. For these transmission measurements, freestanding thin film samples containing scandium ranging from 50-500 nm thick were studied. The scandium thin films were protected by thin films of silicon to prevent oxidation or other potential contamination when removed from the vacuum chamber. From these measurements, the optical constant k was determined, and Kramers-Kronig analysis was performed to determine n.[19]

2.3 Considerations of Scandium Oxide

Each of the studies of scandium thin films mentioned above acknowledge the activity of scandium and its tendency to form compounds with neighboring materials, or an oxide from exposure to atmosphere. Indeed, from the original 1998 Uspenskii paper, it is evident that compound formation at an interface can potentially spread beyond the immediate interface region. Two of the studies

mentioned made attempts to protect or isolate the scandium thin films (particularly from being able to react with silicon) by using a capping or barrier layer. However, little was written to show that this precaution did not introduce a new compound of its own at the scandium interface. For example, the use of tungsten thin films as a buffer layer between scandium and silicon thin films in the 2002 Seely Uspenskii paper may have unintentionally introduced a new compound at the scandium interfaces (there is no mention of whether this issue was investigated). The work done by Larruquert et al. made the greatest effort to ensure the purity of the scandium thin film samples by measuring in-situ over a portion of the energy range of interest thereby avoiding exposure of their samples to ambient atmosphere. Despite such care, these scandium thin films were deposited on a carbon film, at which interface the potential for a scandium carbide compound exists. Films that were to be measured outside of the deposition chamber were capped with a carbon film as well.

An elemental depth profile by either x-ray photoelectron spectroscopy or time-of-flight secondary ion mass spectroscopy may be helpful in confirming or denying the presence of some unexpected compound, though the detection and identification of such a compound would be pushing the limits of such characterization techniques. Similarly, cross-sectional imaging of samples with High-Resolution Transmission Electron Microscopy (HRTEM) would allow insight into the nanoscale physical structure of the coatings studied, and also verify sample quality. However, except for the original Uspenskii paper, none of the studies of scandium thin films cited above employed either of these techniques.

The use of a barrier layer to protect a thin film of interest is certainly a potential solution to maintaining sample purity. In fact, this idea was partially explored as a possible project topic for this dissertation. Consulting binary phase diagrams for scandium showed vanadium to be an excellent, immiscible candidate for partnering with scandium. As part of a preliminary study to test the feasibility of such a project, several Sc/V multilayer coatings were deposited on silicon substrates. Near-grazing reflectance measurements using an x-ray diffractometer provided evidence that these samples have distinct interfaces, and HRTEM imaging of the cross section of the coating confirmed that there was no elemental mixing or compound formation at the interfaces. Again, these were results of preliminary studies where the effectiveness of vanadium thin films to prevent the oxidation of scandium was not fully tested.

In light of recent publications of experimental work with scandium thin films, though, the scandium-vanadium multilayers project was halted. During much of the scandium-vanadium project, the oxidation of scandium had been the issue receiving the majority of attention, specifically the growth process and oxide formation rates. Already having this experience made the study of scandium

oxide a natural project focus. In fact, with subsequent thought to the matter, several advantages to studying scandium oxide became apparent.

Foremost, there is the possibility that scandium oxide thin films may have optical properties that are similar enough to those of scandium that it may serve as an alternative to scandium for highly reflective coatings in the EUV. With the work that has been done with scandium thin films for use in highly reflective coatings, there is still a gap between its measured and predicted reflectivities.[9, 15] The limiting factor to scandium's optical performance may be maintaining the purity of the thin film. Should scandium oxide be able to perform as a "substitute", this purity issue would be avoided.

Secondly (as alluded to by the previous paragraph), scandium oxide exhibits great chemical stability: it has a melting point of 2485 degrees C (which testifies to the strength of the scandium oxygen bonds), and exists as only one species, Sc_2O_3, in the bixbyite structure.[6] These properties of scandium oxide would greatly simplify its study when compared to the issues encountered with scandium thin films. Scandium is quick to bond with other elements because it has three loosely bound valence electrons. Once bound with oxygen, however, these outermost electrons are strongly bound with oxygen which greatly diminishes the possibility of further chemical reaction.

A final justification for studying scandium oxide is simply to contribute to the understanding of material behavior in the EUV. As a material that has never been experimentally studied in the EUV, it would be enlightening to study its optical properties. Recall that the EUV is a young, active area of current research. The optical properties of compounds are needed throughout the UV and EUV. In particular, studying oxides that form readily under ambient conditions (as scandium oxide does) may show a pattern between the optical constants of a compound and those of its constituents. Such a relationship would offer new insight to the optical properties of compounds and is a goal worth pursuing. Also, a serious study of materials in the EUV will contribute not only knowledge about the examined material, but also further develop the experimental techniques and processes. Since the EUV is still a complex and relatively unexplored area, there is great opportunity for new data acquisition methods to be developed, as well as for new insights into the nanoscale structure of materials to be gained. In fact, this study of scandium oxide thin films resulted not only in a measurement of optical constants in the EUV, but also in the development of a novel data collection procedure, as well as a new method for analyzing the data which is notably different from methods used by other researchers in this field.

elements detected	ppm
Aluminum	300
Iron	300
Copper	70
Silicon	70
Calcium	50
Yttrium	20
Nickel	20
Magnesium	10
Silver	1
Manganese	<1

Table 1: Depostion of scandium oxide thin films is performed with DC magnetron sputtering, using a scandium sputter target in an oxygen enviornment. This table shows the results of elemental analysis of the scandium target performed by the manufacturer.

3 Film Deposition

Thin films of scandium oxide are deposited on silicon, quartz, and silicon photodiode substrates using DC magnetron sputtering. The sputter target is 99.9% pure scandium. Table 1 shows the results of chemical analysis performed on the sputter target by the manufacturer, First Reaction.[20] The values reported, in parts per million, are the results from DC Arc Optical Emission Spectroscopy performed on the raw material prior to production.

The vacuum chamber is pumped to ultrahigh vacuum, with initial pumping done by a mechanical roughing pump, followed by use of a cyropump. Generally, the chamber achieves a base pressure of at least 6 e^{-6} Torr after a total of six hours of pumping. A shutter over the opening of the gate valve is then partially closed to reduce pumping speed, and high-purity argon gas is leaked into the chamber through a mass flow controller. The flow of argon is adjusted so that the total vacuum of the chamber is 1-3 mTorr. Figure 1 shows a diagram of the sputter process. In this figure, the sputtergun and sputtertarget are identified by *a,* and the sample platform by *d*, on which the substrates to be coated are mounted. By placing the sputtergun (and sputter target) at high voltage (approximately 2.4 kV) with respect to the vacuum chamber (which is grounded), a plasma is established inside the chamber as the atoms of the argon gas become ionized, nebulously represented by the cloud *b*. The argon ions are accelerated into the sputter target, and the collision between these ions and the atoms on the surface of the target material is sufficient to dislodge atoms from the target and set them adrift in the chamber. In Figure 1, the deposition atoms leaving the target are represented by

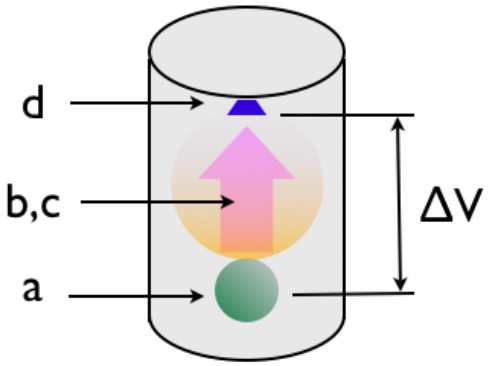

Figure 1: This diagram represents the sputter process. The sphere, *a*, is symbolic of the sputtergun and sputter target. The chamber is pumped to high vacuum, and argon gas is introduced. When high voltage is applied between the sputtergun and the sample platform, *d*, the argon present in the chamber ionizes and becomes a charge carrier. The ions of the argon plasma are accelerated into the sputter target, and the collisions result in atoms of scandium drifting away from the target, represented by the large arrow *c*. In addition to argon, oxygen gas is also introduced to the chamber, represented by the cloud, *b*, through which the scandium atoms travel on their path to coat the substrates on the sample platform. In passing through the oxygen cloud, the scandium forms scandium oxide, so that the film deposited on the substrate is scandium oxide.

the arrow *c*. At this point, the film being deposited is scandium. By introducing oxygen gas into the chamber, the film being deposited is instead scandium oxide.

3.1 Substrates

As mentioned earlier, there are three substrates available for coating. Polished <100> silicon wafers are the standard for normal use. Fused silica, Corning Type 7980, is used for studies which benefit from transmission measurements in the visible. Deposition of films on silicon photodiodes, model AXUV-100 from International Radiation Detectors, Inc, allows for simultaneous reflection and transmission measurements to be made in the EUV.

3.1.1 Polished Silicon Wafers

Silicon wafers are the standard substrate on which films are deposited. A variety of polished silicon wafers have been used in the studies by the BYU Thin Films Group over the years, and it has been found that the best results are had when new <100> wafers are used. Alternatives have included <111> silicon wafers, reclaimed (recycled) wafers, and older, yet unused, silicon wafers. Each of these alternative substrates would, more often than not, have unwanted surface features that would complicate analysis of the deposited film.

Silicon wafers with a <111> orientation are not smooth at the nanoscale. When these surfaces, both bare and coated, were measured with the AFM, a pattern would appear in the images, on the order of roughly 10 nm in height and distributed roughly every 0.4 microns. Figure 2 shows an AFM image exhibiting these features. The image represents the surface of the sample, as seen from directly above (but on the nanoscale). This image was taken using a technique developed in the BYU Thin Films Group which allows for a physical measurement of the film's thickness. Here, though, this technique allows for the topography of the surface of the film as well as the substrate to be identified.[21] The left half of the image in Figure 2 is coated with a thin film of scandium, while the right half of the image is the bare substrate. On the surfaces of both the substrate and the film, the features of interest appear in the form of a triangle with slightly rounded sides and dull corners.

Reclaimed wafers are silicon substrates which were donated to the Thin Films Group by other research groups, but have an unknown history, There have been undergraduate projects that have investigated cleaning, processing, and characterizing these wafers so that they would be suitable for less critical depositions. However, on a majority of these substrates surface structure of an unknown origin could be seen, and with the few reclaimed wafers that were coated for new experiments, ellipsometric measurements and XPS spectra did not analyze in a straightforward matter.

I found older wafers to have a noticeably dirtier surface (regarding nano and micron scale dust, and hydrocarbon contamination), which would interfere with AFM and XPS measurements. Typically, storage of the wafer boxes in a lab space in the underground lab would result in these dirty surfaces over time, while wafer boxes which were kept upstairs in an Eyring Science Center office remained much cleaner (regarding both dust and hydrocarbons).

Excellent surface quality is consistently found among newer silicon wafers, which are minimally handled, stored in the factory case, and sealed inside a plastic bag. AFM sessions using wafers stored in this way did not suffer problems due to surface contamination of dust nearly as much

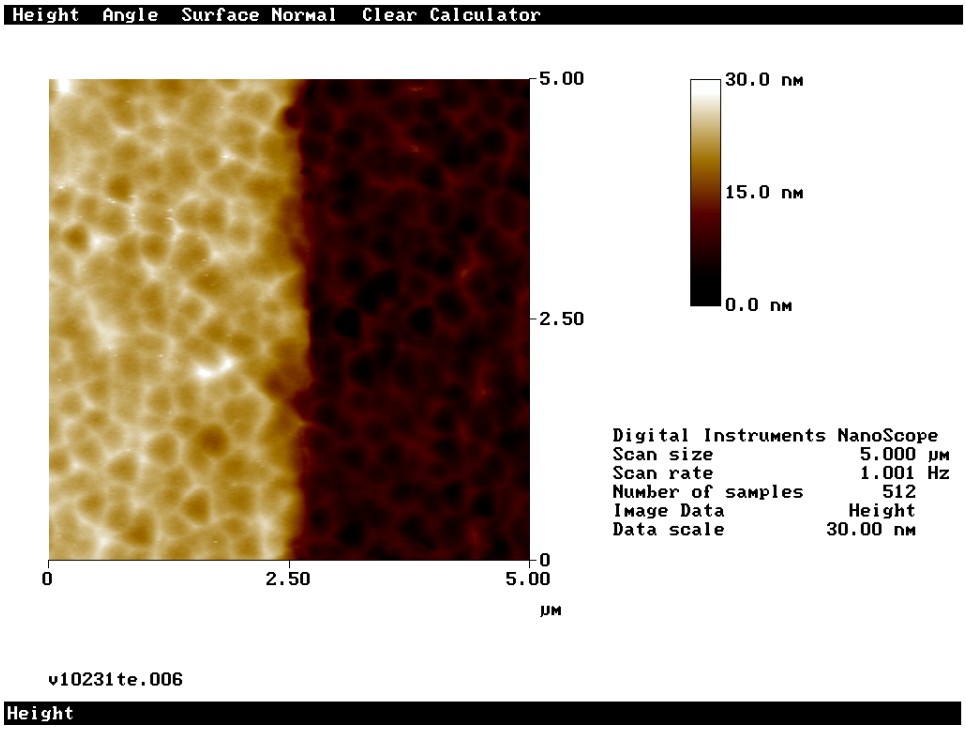

Figure 2: The surface of silicon wafer with a <111> orientation, partially coated by a thin film is shown in an AFM image. To interpret the image, imagine looking down on the surface from above. Features which appear brighter stand taller off of the surface and are closer to the viewer, while darker features are farther away. The left half of the image is coated with a thin film, while the right half of the image is the bare substrate. In this image, the appearance of a triangular shape with rounded sides is noticed in both the region coated by the film and that of the bare substrate. This feature is attributed to the <111> orientation of the silicon wafer used as a substrate.

when compared to wafers stored with less care. Measuring the thickness of the silicon dioxide that is naturally present on these substrates is routinely done using ellipsometry. The silicon dioxide thicknesses are usually in the range of 1.7-2.2 nm, though any value greater than 1.9 nm is attributed to the presence of hydrocarbon contaminants. I noticed that when a new batch of wafers arrive from the supplier, the silicon dioxide thicknesses cluster around 1.75-1.8 nm. As time passes, though, the thickness values seem to grow, even though the amount of silicon dioxide present is undoubtedly constant. The ellipsometer is unable to distinguish between a) silicon dioxide and b) silicon dioxide with a small amount of hydrocarbon or nanodust on its surface, and, as a result, reports the layer of silicon dioxide with the contaminant to be thicker than it truly is.[?]

3.1.2 Fused Silica Slides

Fused silica substrates are used primarily with transmission measurements made with the ellipsometer. A coated piece of fused silica can also be used for reflection measurements as well. For the sample to provide the best reflection data, though, the substrates will need to be properly prepared so that backside reflections are minimized. This is done prior to the substrate being coated. A jig has been machined for roughening (with coarse sandpaper) one side of the substrate not being coated to reduce backside reflections, as illustrated in Figure 3. Jig design acknowledges the need to minimize contact with the surface intended to be coated, and has a channel machined down its center so that the slide is supported only by its sides. By only roughening half of the backside of the slide, the substrate can be used for reflection measurements, as well as straight through transmission measurements.

The slides have dimensions of 3x1 inches, though standard practice is to cut the slide down to 1.5x1 inches. The jig used to hold the slide for backside roughening also proves helpful in holding the slide as it is scored so that it can be sized down.

3.1.3 Silicon Photodiodes

The use of silicon photodiodes as a substrate has become a standard method of sample preparation when studying a thin film in the EUV, as it greatly facilitates the collection of transmission data from a thin film.[22, 16] Additionally, the coated photodiode can also be used for reflection measurements. In this study, the photodiodes used are model AXUV-100, available from International Radiation Detectors, Inc. These detectors are manufactured in batches. Among the diodes from the same wafer

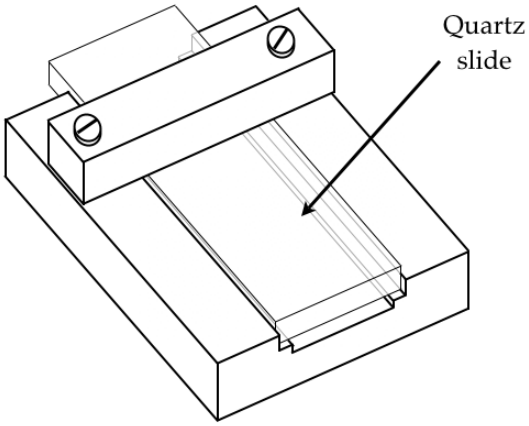

Figure 3: This jig was designed to securely hold quartz slides while preventing contact with the downfacing surface. Slides held in the jig are roughened with sandpaper to minimize backside reflection. Films are deposited on the protected face of the slide, which is facing the base of the jig in the illustration.

of a single batch, it is presumed that all will have an identical history of exposures in the coating and growth processes. Studies of uncoated diodes from the same batch revealed that detector response versus wavelength was nearly identical over a large spectral range (5-18 nm), though at shorter wavelengths (2.5-4 nm) there can be a large difference, as much as 5%, among the individual diode responses. To accommodate for the individuality of each diode, it is best to measure the transmission of a diode before it is coated so that signal versus wavelength data of the bare diode can be referenced later.

Ellipsometry of the AXUV-100 detectors reveals 6.5-6.7 nm of silicon dioxide on their surface. This is in agreement with values suggested by the supplier, as well as thicknesses accepted by other researchers using this model diode.[16, 19]

3.1.4 Substrate Summary

Most deposition of thin films is done on polished silicon wafers. For most characterization techniques (AFM, XRD, and ellipsometry), these substrates are excellent. Fused silica substrates are used when visible and near UV transmission measurements of a thin film need to be done, most likely using an ellipsometer. To optimize the use of this substrate, a portion of its backside should be roughed before it is loaded into the deposition chamber. This can take as much as an hour (setting up the

jig, roughen surface, and cleanup), so it is best to plan on cutting and preparing several fused silica slides at once. Silicon photodiodes are used sparingly and with great care, given their expense. Coated photodiodes are intended for use at the Advanced Light Source Beamline 6.3.2, where their EUV reflection and transmission are measured. In the future, however, it may be possible for such measurements to be made with the monochromator available in the BYU Physics Underground Lab. A jig has been machined to support the photodiodes so that ellipsometric measurements can be made of coated photodiodes to further characterize the deposited film.

4 Film Characterization

Ideally, the films deposited and studied would have the simplest structure and highest possible quality. A film of this perfect nature would have the following attributes:

- Uniform composition, particularly as a function of depth
- Perfectly uniform thickness across the entire surface of the film
- Uniform density over the entire volume of the film
- Smooth, distinct interfaces a) between the film and substrate and b) between the film and vacuum.

However, due to the realities of the geometry of the deposition system, the methods used, and the resources available, the true film structure and quality are often complicated by issues of polycrystallinity, varying elemental composition, and interface and roughness issues.

In this chapter, the characterization of the films is discussed in terms of structure, composition, and quality. The structure of a film refers to a sample's crystallinity, where uniformity is a concern. Film composition refers to its elemental makeup, particularly in regards to depth dependence. Lastly, the quality of a film takes into consideration the film density, the distinctness of the interfaces between different materials, and the amount of surface roughness. Several scandium oxide thin film samples were examined to determine their structure, composition, and quality. Each of the samples were found to have similar composition, though there were differences among them when considering film structure and quality. In Chapter 6.1, a detailed analysis is presented for a single coating.

4.1 Structure

HRTEM was used to study thin films of scandium oxide, with the samples prepared to reveal a cross section. For HRTEM imaging, samples must be thin enough to allow the incident electrons to pass through the sample. There are several methods by which samples can be prepared. A common preparation process is illustrated in Figure 4. Part *a* represents a substrate coated with a thin

film. In part *b*, pieces of scrap silicon are glued above and below the sample of interest to form a "sandwich". The "solid state sandwich" is cored, with the axis of the cylinder running as close along the surface of the thin film as possible. Though not shown, this cylinder is then glued into a copper sleeve for additional strength. Part *d* shows the cylinder after being sliced. A single slice would be mechanically polished on one side until visibly transparent, but shy of wearing through. Final ion polishing is performed on the other side of the sample, until the center of the sample barely begins to erode away. With luck, the portion of the sample that remains around the eroded perimeter will be thin enough to image with the TEM, and also contain the thin film of interest.

Once prepared, samples can be studied by HRTEM, as well as used for Energy Dispersive X-ray analysis (EDX) and Scanning Transmission Electron Microscopy (STEM) studies, described in Sections 4.2 and 4.3.

Initial HRTEM images of scandium oxide thin films show the samples to be polycrystalline. Several films, deposited on both silicon wafers and silicon photodiodes, were studied, and all of them featured this polycrystalline property. As an example, Figure **??** is an HRTEM image showing the cross section of a reactively sputtered, scandium oxide thin film. On the left side of the image is the silicon of the substrate, with its telltale atomic planes. To the right of the silicon is a grey band of silicon dioxide, which is amorphous and appears as a hazy region. Next to the silicon dioxide is the scandium oxide thin film. In this portion of the image, patterns can be seen which do not maintain a single orientation. Also, the patterns do not seem to be uniform in characteristic spacing, but it needs to be kept in mind that this image is a superposition of phase information. A pattern seen in the image may actually be a superposition of two or more patterns, depending upon the structure of the sample in the beam path. These are traits attributed to film polycrystallinity.

Since these individual patterns in the scandium oxide portion of the image do not have distinct borders in the HRTEM atomically resolved images, grain size is difficult to establish in images such as Figure **??**. However, with the beam slightly out of focus, more contrast can be seen from larger scale features, though at the expense of resolving the atomic planes. Figure 5 shows two HRTEM images side by side to illustrate this. In the images of this figure, the lower left corner is the silicon substrate, above which is the gray band of silicon dioxide, and the scandium oxide thin film is on top.

Figure 5 also illustrates another issue encountered when interpreting the HRTEM images. In each of the images, it is difficult to identify the true surface of the film. For example, in both images

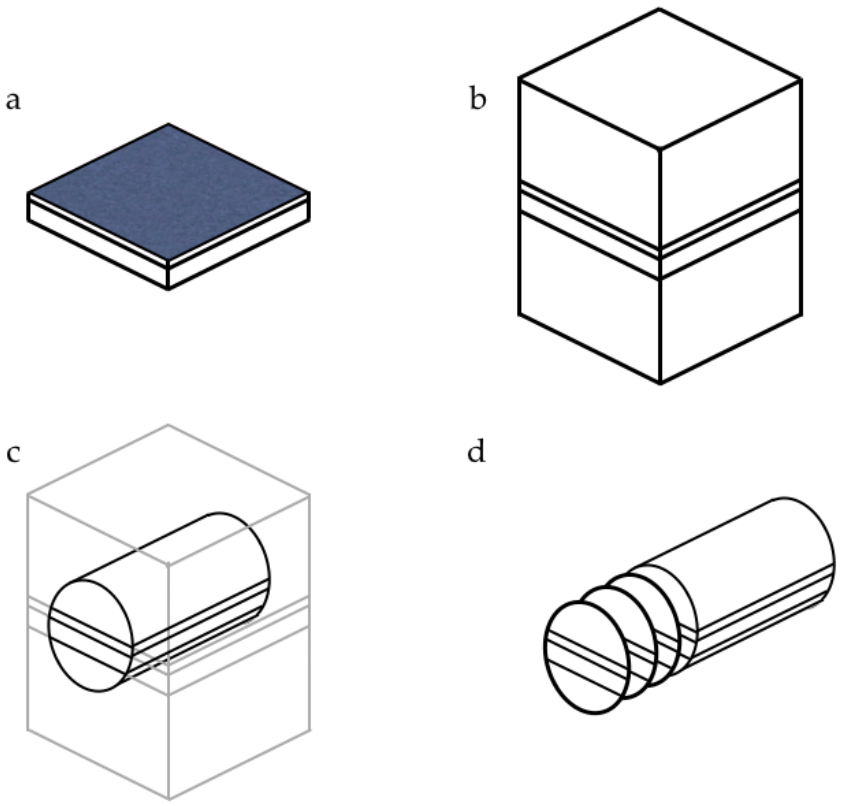

Figure 4: Thin film charaterization by HRTEM, STEM, and EDX requires that the sample be prepared so that electrons can pass through the cross section of the film. Part *a* shows the substrate coated with the thin film of interest. In part *b*, peices of silicon are glued above and below the original sample to creat a "sandwich". The "sandwich" is cored, as shown in *c*. The core is then sliced, illustrated in *d*. One of the slices is selected for further thinning by polishing.

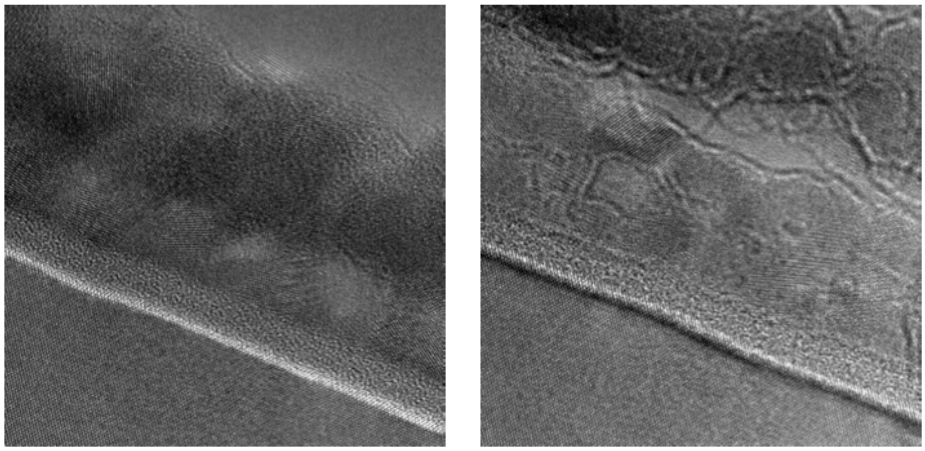

a b

Figure 5: These HRTEM images are of the same portion of a scandium oxide thin film sample. Both images have silicon in the lower left corner, above which is silicon dioxide and a scandium oxide thin film. In *a,* the beam is focused such that resolution is optimized for small scale features such as the atomic planes of the silicon region. Image *b* shows contrast instead among larger scale features, for which the beam was set out of focus.

a and *b* in Figure 5, the top right corners are not part of the thin film, but rather the glue used in sample preparation (as described earlier in this section). The edge that defines the interface of the film surface with the glue is indistinguishable. After inspecting several images, it was concluded that some of the crystalline structures seen at the film surface are not truly part of the film, but instead film material that was removed from the film volume during the polishing of the sample, and coincidentally embedded in the glue layer just above the film's surface. This explanation for the superfluous crystals at the film/glue boundary is supported by STEM data, as described more fully in Section 4.3. With artifacts from the sample preparation process present in the images, using these images to measure film thickness is very difficult. However, useful information regarding sample structure and composition is still available from images collected.

4.2 Composition

Multiple scandium oxide thin film samples were analyzed using EDX during the STEM imaging. In EDX, high-energy electrons collide with the atoms of the sample, causing characteristic x-rays to be emitted. These x-rays are collected by an energy sensitive detector. The measured spectra can be used to identify the presence and relative abundance of specific elements.

To study the composition of scandium oxide thin films versus depth, samples were prepared to reveal a cross section of the film. EDX scans were performed along a line to create a profile that would begin deep in the substrate, moving out past the silicon dioxide at the substrate's surface, into the film, and eventually beyond the film's surface. Figure 6 shows an example of this analysis. The STEM image on the left of the figure shows the cross section of the sample from which the EDX scan is taken. To the right of this image is a line, along which the elemental depth profile is created. The right side of this figure shows the relative intensities of individual elements along the scan line. Reading this graph from left to right, the profile begins by showing only the presence of silicon, as expected, which decays slightly due to the wedge-like shape of the sample. When the scan approaches the surface of the substrate, the silicon signal falls. Immediately the scandium and oxygen signals grow. For the length of the film, the scandium and oxygen signals maintain their relative intensities, and then fall off as the profile leaves the film's surface. Several films were analyzed in this way, on both polished silicon and silicon photodiode substrates. In all cases, the films were found to be composed of scandium and oxygen atoms, without any evidence of unexpected elements in the films.

When the intensities of the scandium and oxygen peaks are monitored versus depth, the ratio of

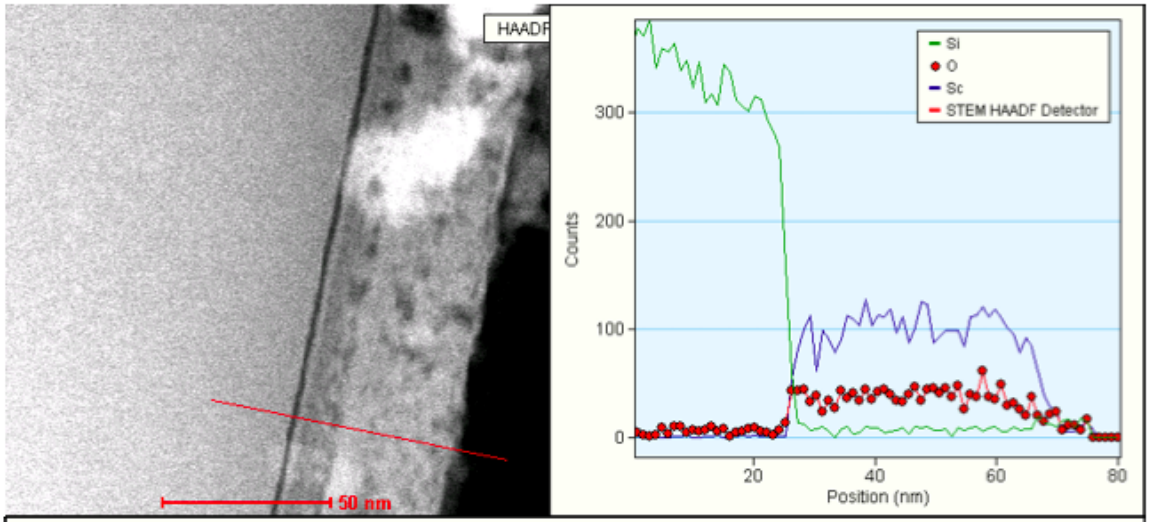

Figure 6: Using EDX, elemental analysis can be performed versus depth. Here, this analysis follows the line seen in the STEM image. The graph to the right shows the presence of elements identified by their characteristic x-ray spectra. This graph shows the presence of silicon deep withing the sample, which falls abruptly as the substrate surface is encountered. At the substrate surface, the oxygen signal rises, as does the scandium signal. The ratio of the oxygen and scandium signal remains relatively constant through the volume of the thin film, after which both signals decay as the probe crosses the surface.

the intensities remains consistent versus film depth. This suggests the composition of the film near the surface is the same as the composition of the film near the substrate. Additionally, a Fast Fourier Transform (FFT) can be applied to selected portions of an HRTEM image to generate a diffraction-type pattern. By selecting a the region of interest for the FFT near the film surface, and another region near the film/substrate interface, these patterns can be compared. It is found that the crystalline structure of the deposited coating is the same at the top of the film as it is at the base.

Since Sc_2O_3 is known to have the bixbyite structure (which is a face centered cubic array of scandium and oxygen, in which oxygen atoms occupy 3/4 of the tetrahedral sites), the FFT-generated patterns provide a means to quickly check whether or not the scandium oxide of a deposited film has the expected phase.[31] Measurements of these patterns indicate the crystals of the film have a lattice parameter of 0.97 nm, which is in good agreement with the value of 0.9869 nm published in a recent x-ray study of the structure of Sc_2O_3 films.[24] To obtain a more precise measurement of the lattice parameter, true diffraction patterns were collected from one of the samples. The lattice parameter from analysis of this pattern, using the silicon <100> pattern of the substrate for calibration, is 0.984 nm.

4.3 Quality

Film quality was determined from Scanning Transmission Electron Microscopy (STEM) images. In STEM, an incident electron beam is scanned across the surface of the sample and detectors collect the electrons that pass through. In the resulting images, the intensity is related to the "mass thickness" of the sample. Mass thickness is the amount of mass present in the portion of the sample that the electron beam is interacting with. This is strongly related to the density of the sample, but as the name suggests, is also influenced by the relative thickness of the sample. When interpreting images, this must be kept in mind since relative intensities from different sample regions may be due to different sample densities, or due to different sample thicknesses. During the sample preparation process, the thin film specimen is thinned by mechanical polishing in a "wedge" shape. As a result, the sample used in the electron microscopy and EDX characterizations of this chapter is progressively thicker in the portions of the sample that are farther away from the tip of the wedge.

Several samples on both silicon wafers and silicon photodiodes have been studied using STEM, with varying results. STEM is very powerful in determining the thickness of a film, even with the

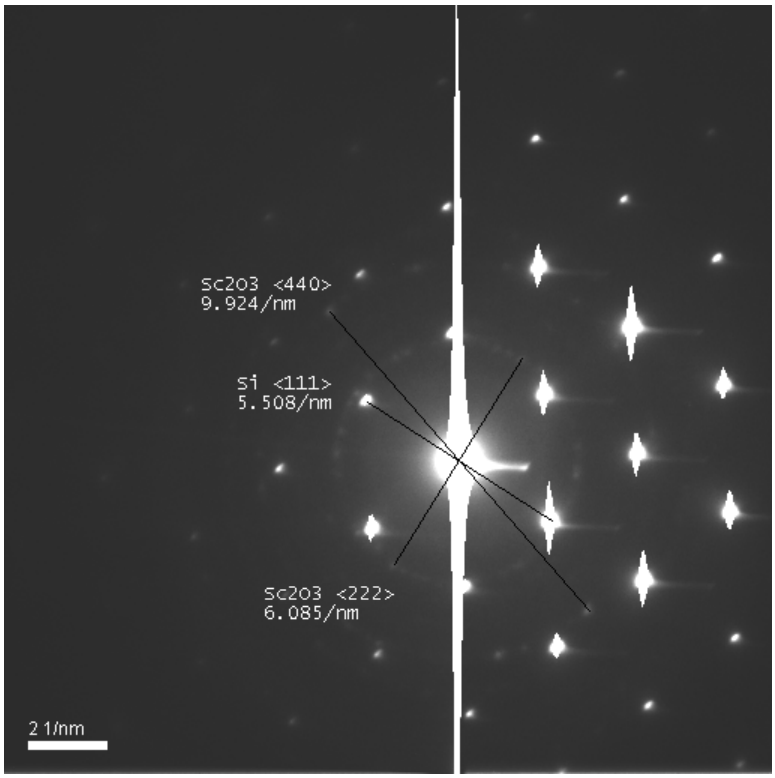

Figure 7: A true electron diffraction pattern from a scandium oxide thin film, collected from the HRTEM. This pattern was analyzed and found the deposited scandium oxide thin film to have a lattice parameter of 0.984 nm, in good agreement with the value of 0.9869 nm from a recent x-ray study of Sc_2O_3.

polishing-produced crystal debris littering the film surface region (as mentioned in 4.1). Unlike the effects these extra crystallites at the film surface/glue interface have in the HRTEM images, the contributions of the imbedded residue to STEM images are easily identified and accounted for in the data collection and analysis. In essence, the presence of the polishing artifacts "washes" out as thicker parts of the sample are examined. This is made possible by the wedge quality of the sample. Features in the image due to the polishing residue will have a lower relative intensity in the images if the sample is examined where the "mass thickness" of the imbedded residue is small relative to the "mass thickness" of the film. Consequently, the STEM images show a surface/glue interface which is distinct, allowing for film thickness measurements to be made with ease.

Since the STEM is very density sensitive, this characterization showed that the films being studied could not accurately be described simply as single layer. None of the samples studied were found to have constant density value versus depth. In fact, Figure 8 shows images from two different samples of scandium oxide thin films, where the top image reveals the coating to be a bilayer, and the lower image is a trilayer.

STEM images are also able to provide information about the film where it is exposed to ambient at the surface. AFM measurements could also be used for measuring the surface roughness of the samples. However, the samples studied were not well suited for this characterization. Once the sample has been exposed to atmosphere for more than a couple of days, it collects enough nanodust on its surface to complicate AFM imaging, as the nanodust will attach itself to the AFM probe. Several methods to clean the surface were considered. Unfortunately, a solution for removing the nanodust which does not introduce new nanoscale contaminants of its own could not be found.

Using STEM for roughness analysis is not common practice. It was found to have a distinct advantage over AFM roughness studies since cross sectional STEM images also reveal information about the interfaces below the surface. When image intensity is displayed versus depth, the interface regions are easily identified. The slope of the intensity profile in the interface region shows how quickly the sample transitions from one material to the next, which is directly related to roughness. Since silicon dioxide and silicon are so well studied, their interface provides a standard to which other interfaces can be compared. This technique of using the intensity profile from an STEM image to study interfacial roughness below the surface is a novel approach, though it is still being developed.

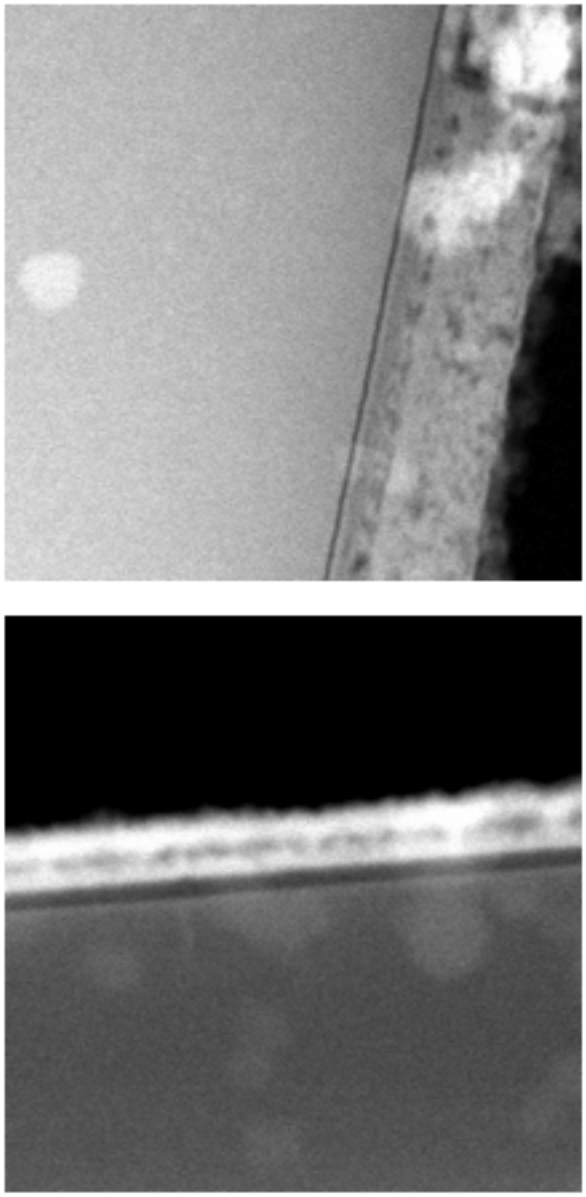

Figure 8: STEM images of two different scandium oxide thin films samples reveal that the coatings deposited are not simple monolayers. In the upper image, the thin, dark vertical stripe is silicon dioxide. To the left of this is silicon, and to the right is the scandium oxide thin film (dark and light grey bands) and the glue used in the sample preparation (black). In the lower image, the bottom region is silicon, above which is a layer of silicon dioxide, and the scandium oxide thin film. In each image, the area associated with the scandium oxide thin film is not uniform in intensity. Since the scandium oxide is the same material throughout its volume, the intensity differences are due to a variation in the density of the materal. In these images, it is certain that the scandium oxide thin films deposited are not a simple single layer.

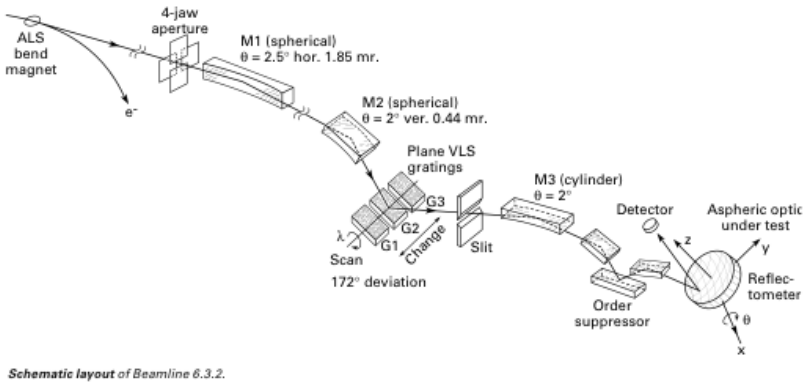

Figure 9: Schematic of ALS Beamline 6.3.2 (courtesy ALS 6.3.2 website).

5 EUV Measurement of Thin Films

Reflection and transmission measurements were made at Beamline 6.3.2 of the Lawrence Berkeley National Laboratory Advanced Light Source (ALS). The ALS is a third-generation synchrotron facility, and Beamline 6.3.2, in operation since February 1995, is designed for high-spectral purity and wavelength accuracy. Light from the synchrotron bend magnet enters the beamline and is deflected horizontally with a spherical mirror. Next, the light beam is deflected by a bendable refocussing mirror, followed by spectral separation using a monochromator (which was designed and constructed by the Center for X-Ray Optics). The high-spectral purity of the photons interacting with the sample is achieved by using a combination of filters and a triple mirror "order suppressor".[25]

Measurements at the ALS are made over the range of 2.7-50 nm. Not all of these wavelengths are available at once, since only a select wavelength range is accessed by using a specific combination of grating, filter, and order suppressor. To measure a sample over the entire 2.7-50 nm range, data is collected in a single wavelength range, then a different combination of grating, filter, and order suppressor are used to collect data in another wavelength range. Table 2 shows the wavelength ranges available and the gratings, filters, and order suppressors appropriate to each one.

The quality of the reflection and transmission measurements relies very strongly on the intensity of the photon beam. When a wavelength range is accessed by a combination of grating, filter and order suppressor, the intensity of the photon beam varies versus wavelength. This gradient is most noticeable among the shorter wavelengths of a given range, since the filter used is absorbing there.

wavelength range (nm)	grating (lines/mm)	filter	order suppressor
2.7-4.8	600	Ti	Ni@6.2 degrees
4.4-6.8	600	C	Ni@8
6.6-8.8	600	B	C@6.2
8.4-11.6	200	B	C@8
11-14	200	Be	C@10
12.4-18.8	200	Si	C@10
17.1-30	80	Al	C@14
25-50	80	Mg	C@20

Table 2: The first column shows the wavelength ranges available at the ALS. The row for each wavelength range shows the grating, filter, and order suppressor choice and position combination used to access photons in that range.

Subsequently, the data among the shortest wavelengths of a collection range can be of lower quality than the data at other wavelengths in that range, due to a poorer signal to noise ratio. Notice, though, that there is an overlap among the individual wavelength ranges. For the portion of a wavelength range where the data (and later, the results from fitting the data) is less desirable, data from a different wavelength range can be utilized instead.

5.1 Simultaneous Reflection and Transmission Measurements

The use of silicon photodiodes as substrates for the thin films being studied has become a standard approach when considering the optical properties of thin films in the EUV.[16] Essentially, the photodiode is a device which outputs an electrical signal when a photon is absorbed. The AXUV-100 photodiodes available from International Radiation Detection, Inc. are tailored to have increased sensitivity in the EUV.[22] By coating one of these diodes with a thin film, any signal reported will be from photons that have traveled to the detector through the thin film as well as the dead layer of the detector surface. The dead layer of the detector is a region between the silicon dioxide of the detector's surface and the silicon of the detector's volume in which no electron-hole pairs are created. From previous work with the AXUV-100 photodiodes, we believe this region to be 1-2 nm thick.[23]

Using photodiodes coated with thin film of interest has greatly facilitated making transmission measurements. Additionally, by employing an auxiliary, uncoated photodiode, reflection measurements can be made of light having bounced off the surface of the coated diode. This concept is illustrated in Figure 10. Notice for incident energy to be conserved, there are only three possibilities of where the photons may exist after they have interacted with the film:

1. As part of the reflected beam.
2. As part of the transmitted beam.
3. Absorbed into either the material of the thin film or the dead layer of the detector.

This conservation of energy assumes the efficiency of the photodiodes used for photon detection to be perfect. IRD claims that their detectors do indeed have 100% quantum efficiency.[22] Skeptical of such a claim, several EUV measurements have been made with bare IRD AXUV-100 detectors while at the ALS. The ability to truly measure the efficiency of the detectors, though, is a challenging project and not easily solved with the resources and time available. A greater concern was that of the consistency of detector response when comparing one to another. It was found that the individual responses don't match exactly, but instead deviate by as much as 5% in certain energy ranges.

A novel approach to collecting this reflection and transmission data from a coated diode is to make both data collections simultaneously. This approach had not been attempted before, even though it was implemented with relative ease. A new sample stage was designed for use in the ALS vacuum chamber, illustrated in Figure 11. This new stage holds the coated diode while transmission measurements are made. Its design allows light reflected from the coated diode's surface to travel uninterrupted. The positioning system already in use inside the ALS vacuum chamber allows the sample stage to be rotated to any angle θ (relative to the incoming beam), as well as locate the reflection detector to the corresponding specular angle, 2θ. Of particular interest are the angles a) θ=90 degrees, where the coated diode is positioned with its surface normal to the beam, and b) $0<\theta<25$ degrees, (known as near-grazing angles). The design of the new stage maximizes the angles available in this near-grazing region. However, due to the raised perimeter of the diode's ceramic support base, not all grazing angles are available. It has been found that on average the smallest possible angle where quality data can be collected is about 9 to 10 degrees.

Among the advantages of collecting data in this fashion are:

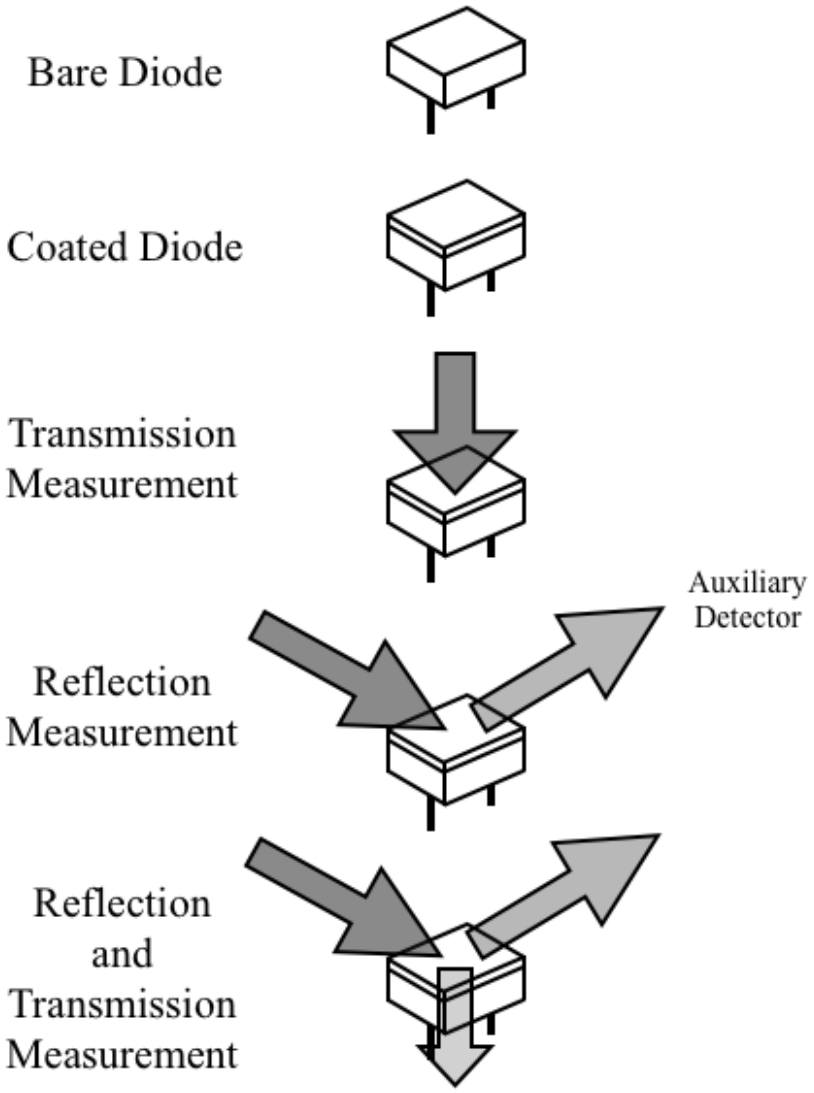

Figure 10: These drawings illustrate the use of silicon photodiodes used as substrates for reflection and transmission measurements of thin films.

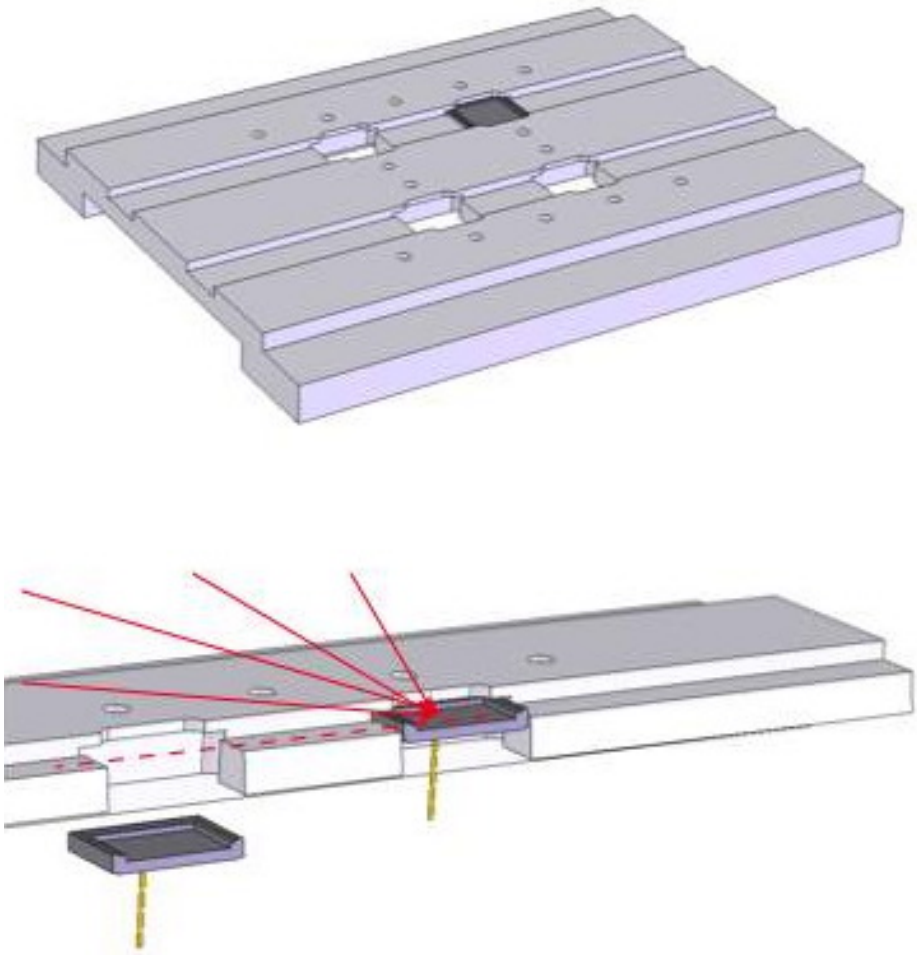

Figure 11: The new stage designed to accomodate simultaneous reflection and transmission measurements has a trough machined in its surface to allow light near-grazing to approach the coated diode uninterrupted. In the cross sectional view, incident light at various angles is represented by vectors, while the grazing incidence path is shown with the dashed line. It can be seen that the raised perimeter of the diode's base limits the angle nearest to grazing available.

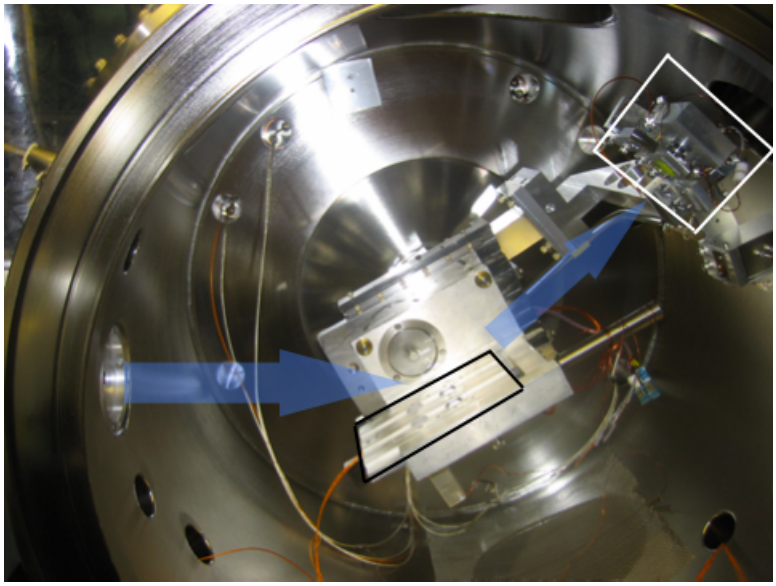

Figure 12: This picture of the ALS vacuum chamber shows the orientation between the stage holding the coated photodiode and the array of detectors for reflection measurements (both are outlined with boxes). The light arrow to the left of the sample stage shows the path of the incident light beam, while the light arrow to the right of the sample stage represents photons reflected from the sample surface.

- The reflection and transmission data come from exactly the same part of the thin film coating, and the conditions of the data collection are exactly the same.
- Twice as much data is collected in a given time.
- Since reflection and transmission trade off in amplitude versus angle (when theta is near-grazing), simultaneous analysis of both data sets may prove more powerful than previous approaches of modeling reflection or transmission individually.

It should be recognized here that the data as collected is not in its simplest form for analysis. Each scan measured the reflection (and transmission) data with the sample at a specific angle, while the changing wavelengths of the incident photons. From a computation perspective, this is a very complex situation to describe, since the optical constants of each of the materials (high-density scandium oxide, low-density scandium oxide, silicon dioxide, and silicon) will be different at each wavelength of the scan. A preferred form for the data to have is a measurement of reflection (or

transmission) of a single wavelength of light, over a range of angles. One of the realities of data collection at the ALS is that measurements of this kind, $\Theta - 2\Theta$ at a single wavelength, are more problematic (e.g. the goniometers have a tendency to hang and not respond to software commands). However, this issue is resolved by using a computer program which takes a batch of files (from a single wavelength range) which covers a large range of near-grazing theta values, and assembles a single matrix to represent all this data for the wavelength range. From this matrix, the program assembles new files with the reflection and transmission data for each wavelength of the range, versus theta.

Once the data has been compiled in this fashion, such that each file corresponds to a specific wavelength with reflection and transmission signals each expressed versus theta, the data is normalized to give absolute reflectance and transmittance. The following equations show the steps by which the measured signals are processed to provide reflectance and transmittance values:

$$R = \frac{\frac{\left(A_R^j - A_D^j\right)}{I_R}}{(10^{k-j})\frac{\left(A_S^k - A_D^k\right)}{I_S}}$$

$$T = \frac{\frac{\left(C_T^l - C_D^l\right)}{I_T}}{(10^{m-l})\frac{\left(B_S^m - B_D^m\right)}{I_S}}$$

In these equations, the signals from three different detectors used are represented by A (ALS diode), B (bare diode on the sample stage), and C (coated diode on the sample stage). The subscripts denote whether the signal is: reflected from the coated diode (R); transmitted through the sample to the coated diode (T); measured from the uninterrupted (or straight through) beam (S); or associated with no incident photons at all (D, for dark). The superscripts specify the gain setting on the preamplifier at the time of the data collection. In the denominators, the scaling factor 10^{p-q} accounts for the possibility that reflection or transmission data may be collected at different gains than the straight through data. An example of the data digested in this way is shown in Figure 13.

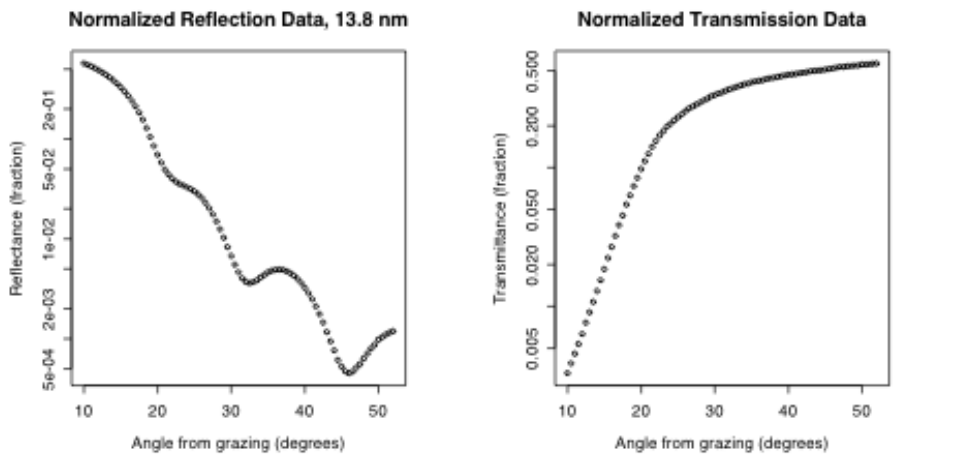

Figure 13: The two graphs show examples of reflection and transmission data of 13.80 nm light that has been normalized. In the reflectance data, interference fringes easily seen.

6 Sample Sc0305

The experimental studies of scandium oxide thin films culminated in the EUV measurement of a scandium oxide coated photodiode. During the film deposition, three substrates were present on the sample platform: a polished silicon wafer, a fused silica slide, and a silicon photodiode. These substrates were coated and named Sc0305 Witness, Sc0305 Quartz, and Sc0305 Diode, respectively. This chapter is dedicated to the characterization of Sc0305 Diode by HRTEM and STEM, and the description of the film's physical traits.

Sc0305 Witness was used for ellipsometric measurements and imaged using HRTEM and STEM. Similarly, Sc0305 Diode was also measured with ellipsometry, HRTEM, and STEM, as well as being used in EUV reflection and transmission measurements at the ALS.

Upon inspection of Sc0305 Witness, it could be seen that the film thickness was not uniform over the length of the sample. This was evident in the gradient of the surface coloration. Given the geometry and design of the deposition chamber, this thickness variation was not surprising. However, since the optical measurements would be taken with a beam whose cross section is less than a millimeter, the nonuniform film thickness was not expected to complicate data analysis.

6.1 Electron Microscopy Characterization of Sc0305

HRTEM images of both Sc0305 Witness and Sc0305 Diode showed that this coating is a polycrystalline bilayer (Chapter 4). Figure 14 is an example of a high-resolution image of this coating, taken from Sc0305 Witness.

Images collected slightly out of focus revealed the grain boundaries, identifying crystallites with two different approximate sizes, localized to different portions of the film. This is illustrated in Figure 15. The far right portion of the image is the glue layer above the surface of the film. Crystallites are seen on both sides of the film/glue interface. Those on the glue side are polishing residue imbedded in the glue (see Section 4.3). To the left of the film/glue interface is the bulk of the film, in which large crystallites can be seen. The size of the grains of these crystals is difficult to discern, as their boundaries are not easily identified. Continuing towards the upper left corner another interface is seen, with more crystallites on the left side. On each side of this interface is scandium oxide. Here, too, the size of these crystal grains is also difficult to measure, but it is recognizable that they are considerably smaller than those to the right. This localization of small and large grains to the lower and upper portions of the film (respectively), together with a noticeable interface between the two regions, suggests that the Sc0305 coating is a bilayer. In the images, the lower layer of the Sc0305 Witness sample is approximately 12-13 nm thick, while the upper layer is about 36-38 nm thick.

As explained at the beginning of this chapter, the film deposited on the substrates varies in thickness due to the geometry and design of the deposition chamber. With this in mind, the images from Sc0305 Witness are useful to establish the structure and quality of the film, but information about the film thickness for use in EUV data analysis is best taken directly from Sc0305 Diode. The HRTEM and STEM imaging is helpful in providing an estimate for the film thickness, but is not the best method of characterization to determine the exact thickness value. This is because the image is of only a single location of the coating face, which may be far removed from the portion of the sample interacting with the EUV photons when reflection and transmission measurements are taken.

Following the EUV data collection at the ALS, the coated photodiode was sacrificed for cross sectional electron imaging. As shown in Figure 16, Sc0305 Diode also exhibits the bimodal quality seen in the images of Sc0305 Witness. Here, though, the lower layer is substantially thinner, and has an approximate 1:10 ratio with the upper layer. It is not surprising that the total film thickness of Sc0305 Diode is different than that of Sc0305 Witness, but it is unclear how the bilayer ratio could

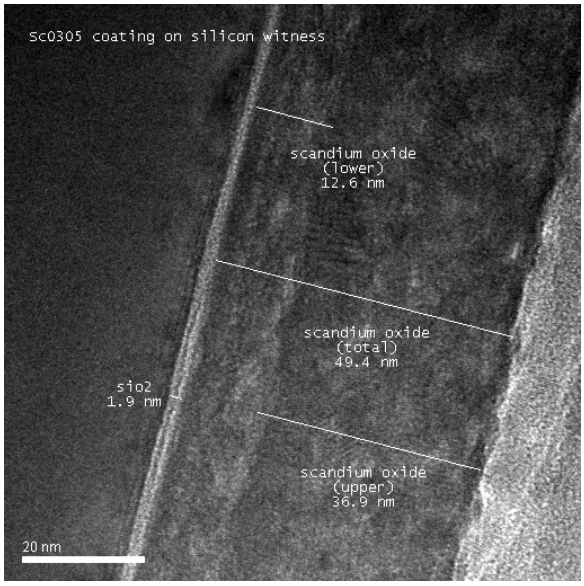

Figure 14: An HRTEM image of Sc0305 Witness shows this coating is a bilayer. The upper layer of the coating has larger grains present that the lower layer.

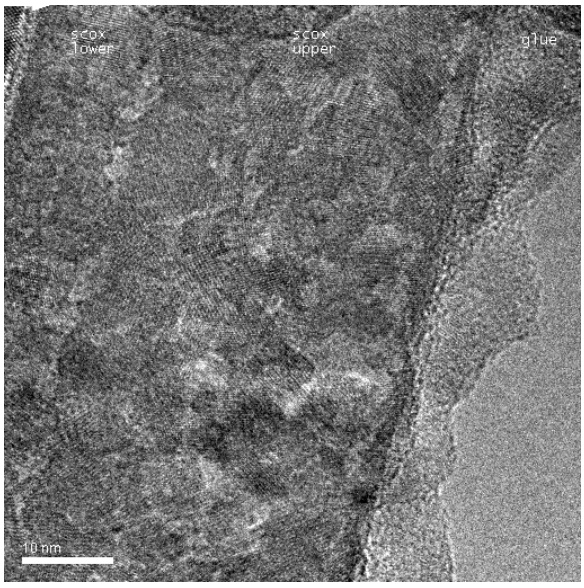

Figure 15: The distribution of the crystallites in Sc0305 is more evident in this HRTEM image collected with the beam slightly out of focus and at a greater magnigication. Larger crystallites are seen in the upper layer of the scandium oxide bilayer.

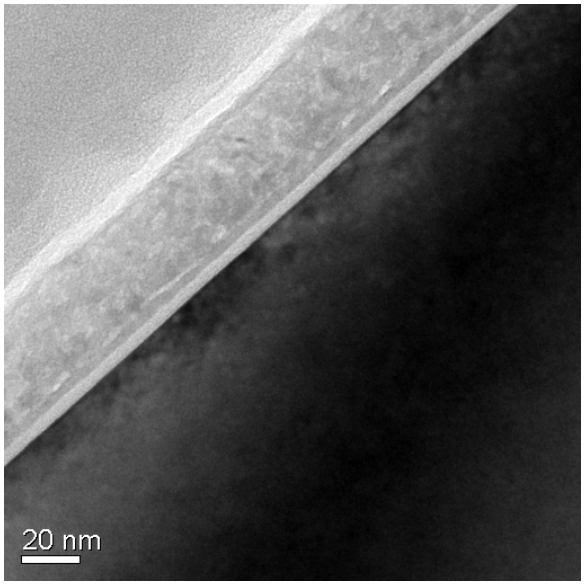

Figure 16: The bilayer structure of the scandium oxide coating found in Sc0305 Witness is also seen in this HRTEM image of Sc0305 Diode.

differ between the two samples. From the HRTEM images, the total thickness of Sc0305 Diode is estimated to be about 35 nm.

With the HRTEM images suggesting that the Sc0305 coating is a bilayer, STEM imaging on Sc0305 Witness was performed. STEM imaging of Sc0305 Diode was planned as well. However problems with the TEM which has the STEM and EDX capabilities have put that imaging session on an indefinite hold. An immediate query was whether or not the lower film was correctly identified as scandium oxide. From a practical point of view, there was conceivably very little that it could be otherwise, since the only sputterable material in the chamber was scandium (except the accumulated coating on the chamber walls, but that is not subject to energetic collisions with the argon ions). The EDX elemental depth analysis of Figure 6 presented in Section 4.2 was done with Sc0305 Witness, and found that the deposited scandium oxide film was composed only of scandium and oxygen.

The EDX analysis and the corresponding STEM image are presented in Figure 17. On the right is the intensity profile taken along the line selected in the STEM image. Recall that STEM images associate a greater intensity with regions in the image where the "mass thickness" of the sample is greater. From the intensity profile in Figure 17, the lower portion of the film is found to have a lower density, which is sensible given that the HRTEM images found that the crystal grains in this region are smaller than those in the upper portion of the film. Smaller grains results in more voids

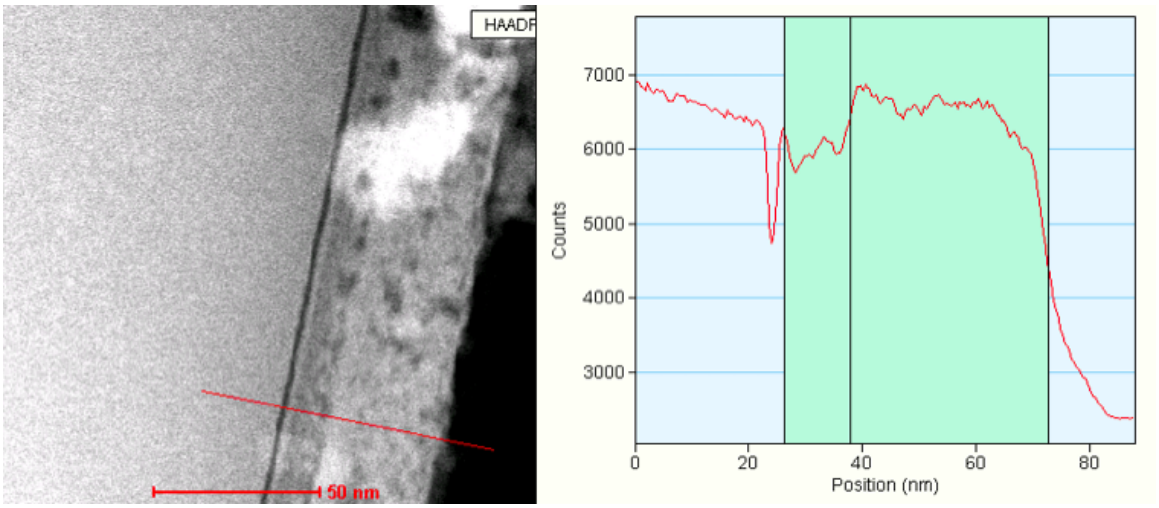

Figure 17: EDX analysis can be performed along a specified path. At the bottom right of the STEM image is the path which corresponds to the intensity profile to the right. This profile shows the dependence the image intensity has versus depth, which in this case reveals that the scandium oxide thin film of this sample is a bilayer.

per unit volume, which is explains the lower density of the lower part of the bilayer with respect to the upper layer. It is estimated from this intensity profile that the lower film is about ninety percent as dense as the upper film.

6.2 Ellipsometry with Sc0305

An M-2000 Variable-Angle Spectroscopic Ellipsometer from the J. A. Woolam Company was used for the ellipsometric measurements. This instrument has a wavelength range of approximately 185 - 1000 nm. Previous studies of reactively sputtered scandium oxide thin films on fused silica had shown that this material is transparent at wavelengths longer than 300 nm. The measured data was modeled using a Cauchy parametric layer to represent the scandium oxide thin film, since a Cauchy layer describes transparent films very well. To optimize the data to work with the model, the measurements outside of the 310-1000 nm spectral range were discarded since this is the region where the scandium oxide thin film is assuredly transparent.

Early analysis of the ellipsometric data was done assuming that the sample was a film of uniform density and composition. Characterization of the coated silicon wafer by HRTEM, STEM, and EDX confirmed that the film did have uniform composition, Sc_2O_3, but did not have uniform density. Not

surprisingly, the values for the film thickness generated in the original ellipsometric modeling sessions did not match those provided by STEM and TEM, since a monolayer model was being applied to the bilayer data.

A second attempt at modeling the ellipsometric data was made after it was learned that the Sc0305 coating is actually a bilayer. In this session, the model was built to accommodate the fact that the two layers deposited above the silicon dioxide were similar in composition, but of different densities. The results of the STEM analysis suggested that the ratio of the densities be such that the lower layer be 90% as dense as the upper layer.

Even before analysis of the ellipsometric data takes place, the relative position of the the peak in the delta data reveals the relative thickness of the film measured when compared to another set of data. For ellipsometric measurements in general, when considering films of an identical material, the peak in psi shifts to lower energies as film thickness increases. Figure 18 shows three sets of data for Sc0305. The psi data shown are measurements made of the Sc0305 coating, both on the silicon wafer and photodiode substrates. The graph of psi data at the top is a set of measurements taken from Sc0305 Diode. Both the data in the middle and at the bottom come from Sc0305 Witness, with each set of measurements taken from different ends of the coated silicon wafer. This figure shows the variation in film thickness that is possible across the sample platform in the deposition chamber. Thus, for analysis of the data taken at the ALS from Sc0305 Diode, it is paramount to establish a thickness of the film that matches as close as possible the portion of the film which was interacting with the photons of the measurement. The film thickness value used in the EUV analysis, then, is best determined from the EUV data itself. Thickness values found through ellipsometry, HRTEM, and STEM can be used to establish a neighborhood in which the true thickness resides.

6.3 Sc0305 EUV Data Collection

Sc0305 Diode was measured at the ALS on two separate occasions. Data collected in the first measurement session of March 2005, however, was superseded by the data collected in October 2006. This is because the new technique for simultaneously collecting reflection and transmission data was still being refined in the spring of 2005, and the data collected at that time suffers from excessive noise in the transmission signals. Data collected in October 2006, however, has an excellent signal to noise ratio, and also benefits from a fourth grating being available on Beamline 6.3.2, allowing data to be collected from 2.8-50 nm (as opposed to 2.8-35 nm). Data collected on the 2006 trip falls

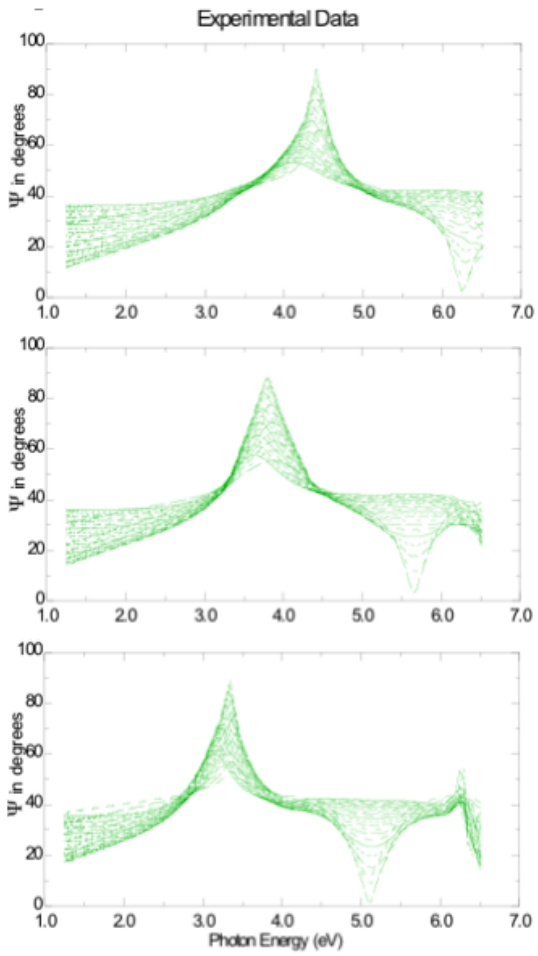

Figure 18: Ellipsometric psi data showing the difference in film thickness among the substrates of the Sc0305 coating. The position of the peak shifts to lower energies with increasing film thickness. At the top is data collected from Sc0305 Diode, followed by data collected from two different locations of Sc0305 Witness. From the geometry of the deposition system, it was expected that the thickness of the deposited film would be nonuniform, as illustrated by the measurements shown here.

into two main categories:

- Transmission versus wavelength, with the sample positioned normal to the incident photons.
- Reflection and transmission versus wavelength, with the sample positioned at an angle near-grazing. The near-grazing angles range from as little as 8 degrees to as many as 80.

In the reflection and transmission versus wavelength measurements (R&T measurements for short), the start and end points of the scan are the shortest wavelength and longest wavelength available from a specific combination of grating, filter, and order sorter. As mentioned in Section 5, the intensity of the beam of photons is not uniform across the entire wavelength range. This results in some wavelength ranges providing better data than others. Also, the wavelength dependence of scandium oxide's n and k make for high-quality reflectance data in some ranges, and low-quality reflectance data in others. Transmission data, too, varies in quality among the wavelength ranges.

In R&T measurements, data was collected while varying wavelength with the sample at an angle, and the reflection detector at twice that angle (in the usual specular path). When this scan was completed, the sample angle was changed some small amount, the reflection detector moved to the appropriate position, and the wavelength scan performed again. This was done beginning with a sample angle of 10 degrees, and continued through a range of angles until the amplitude of the reflection signal diminished to the point that the data quality was unacceptable.

7 The Thickness of Sc0305 from EUV Data

As the EUV reflectance measurements were made, sinusoidal type patterns were observed as the data was appeared on the monitor. In certain spectral regions, away from the wavelengths associated with the electronic transitions of scandium oxide, silicon dioxide, and carbon, the maxima and minima of this pattern would be the dominant features of the scan. With each successive data collection, the sample angle theta would be increased a small amount, and the positions of the maxima and minima would shift accordingly. The pattern of maxima and minima being observed is an interference pattern, due to the constructive and destructive interference of photons reflected from the different interfaces of the sample. An interface exists at the boundary between one material with a certain index of refraction and a material with a different index of refraction. In the Sc0305 Diode sample, there are four interfaces:

- Vacuum with scandium oxide
- High-density scandium oxide with low-density scandium oxide
- Low density scandium oxide with silicon dioxide
- Silicon dioxide with silicon

There are equations to describe this interference pattern. A common equation for interference from a single thin film coating is

$$2nd\sin\theta = m\lambda \tag{1}$$

where n is the index of refraction of the coating, d is the film thickness, θ is the angle of incidence of the photons from grazing, m is a real number identifying the order of the pattern, and λ is the wavelength of the photons creating the pattern.[1] This equation is valuable for developing an understanding of the pattern and the dependence it has on each of the variables. However, in this form it is oversimplified and insufficient to fully describe the pattern, due to common approximations made along its derivation. Still, by using this simple equation to become familiar with interference patterns, some important properties of the patterns can be identified. Foremost is that the spacing between the minima on each side of a specific maximum is unique. That is, in this equation a

maximum appears in the pattern when the parameter m is either a whole or half integer, depending on the total phase change the photon experiences from crossing interfaces. The value of m that is associated with a specific maximum identifies the order of that fringe. Each fringe order will have a unique spacing between the minima neighboring the maximum of the fringe. Interference maxima of higher orders have the neighboring minima closer together than interference maxima of lower orders.

By taking advantage of the order specific spacing among the minima, the interference fringes can be used to determine the film thickness of the coating producing the pattern. Even though at this point the values for the indices of refraction of the scandium oxide thin film are unknown, estimates of their values can be made and used as a starting point for this analysis. Optical constants for scandium oxide obtained from the CXRO database were used as a reasonable starting value. Since scandium oxide is a compound that had not been explicitly studied in the past, the values for n and k from the CXRO website are produced by referencing those present in the database for scandium, which are the values determined by Aquila et al, and "mixing" them with the n and k values for oxygen. This "mixing" is essentially a weighted average, according to the stoichiometry of the oxide, Sc_2O_3. As an approximation of the optical properties of a compound, this approach is generally taken to work reasonably well. However, this method of calculating the optical constants of a compound from its constituents overlooks the changes that will occur among the energy levels of the atoms involved. In particular, the approximation will be less valid in wavelength regions where photoabsorption occurs.

7.1 Matrix Method for Calculating Reflection and Transmission of Thin Films

As an alternative to using Equation 1, calculations were made of the reflectance (and transmittance) of the coating using a matrix method product of Fresnel coefficients representing the reflection and transmission at each interface.[26] Derivation of the Fresnel coefficients is frequently found in optics textbooks. The Fresnel coefficients describing the interface can be expressed in terms of the indices of refraction and the wave vectors of the materials on each side of the interface. For light with s polarization, the Fresnel coefficients used for calculating reflection, f, and transmission, g, at an interface are

$$f_{12}^{s} = \frac{k_{z1} - k_{z2}}{k_{z1} + k_{z2}} \tag{2}$$

$$f_{21}^{s} = \frac{k_{z2} - k_{z1}}{k_{z2} + k_{z1}} \tag{3}$$

$$g_{12}^{s} = \frac{2k_{z1}}{k_{z1} + k_{z2}} \tag{4}$$

$$g_{21}^{s} = \frac{2k_{z2}}{k_{z2} + k_{z1}} \tag{5}$$

The subscripts of f and g specify the direction of propagation of the light being considered. For example, f_{12}^{s} is the Fresnel reflection coefficient for s polarized light traveling from layer 1 to layer 2. In these equations, k_{zi} is the z component of the wave vector, k_i,

$$k_i = \frac{2\pi N_i}{\lambda_0}$$

$$k_{yi} = \frac{2\pi}{\lambda_0} \cos\theta_i$$

$$k_{zi} = \sqrt{k_i^2 - k_{yi}^2}$$

where N_i is the complex index of refraction, and θ_i is the angle of incidence from grazing. The expression for k_{zi} is dependent upon the index of refraction of the ith material, and in turn the Fresnel coefficients for an interface use the indices of refraction of the material above and below the interface.

For p polarized light, the Fresnel coefficients are

$$f_{12}^{p} = \frac{N_2^2 k_{z1} - N_1^2 k_{z2}}{N_2^2 k_{z1} + N_1^2 k_{z2}}$$

$$f_{21}^{p} = \frac{N_1^2 k_{z2} - N_2^2 k_{z1}}{N_1^2 k_{z2} + N_2^2 k_{z1}}$$

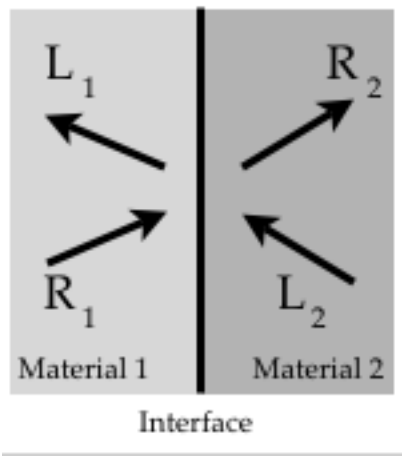

Figure 19: This diagram represents the waves in the materials on both sides of the interface.

$$g_{12}^{p} = \frac{2N_1N_2k_{z1}}{N_2^2k_{z1} + N_1^2k_{z2}}$$

$$g_{21}^{p} = \frac{2N_2N_1k_{z2}}{N_1^2k_{z2} + N_2^2k_{z1}}$$

A full treatment of the use of the Fresnel coefficients to describe the behavior of light in the material above and below an interface is given in the *Validation of Optical Codes*, by R. S. Turley. The derivation culminates in a formulation of a 2x2 scattering matrix, A^q, which represents an interface in a thin film when considering the q polarization of light (either s or p). A^q is used in the equation

$$\begin{pmatrix} L_1 \\ R_1 \end{pmatrix} = A \begin{pmatrix} L_2 \\ R_2 \end{pmatrix}$$

where R_i and L_i represent waves moving to the right and to left in the ith material on either side of the interface. Figure 19 illustrates the interface with the L_i's and R_i's.

The elements of A^s are

$$A_{11}^{s} = g_{21}^{s}C_1C_2 - \frac{f_{21}^{s}f_{12}^{s}C_1C_2}{g_{12}^{s}}$$

$$A_{12}^{s} = \frac{f_{12}^{s}C_1}{g_{12}^{s}C_2}$$

$$A_{21}^{s} = -\frac{f_{21}^{s}C_2}{g_{21}^{s}C_1}$$

$$A^s_{22} = \frac{1}{g^s_{12} C_1 C_2}$$

where C_i is the propagation coefficient, which is a phase and attenuation factor, $C_i = \exp(i2k_i d_i)$, and d_i is the thickness of the ith layer. The matrix elements of A^p have the same form as those of A^s, but using the Fresnel coefficients for p polarized light. To describe the interaction of light with a sample having several interfaces, the product of the scattering matrices representing each interface is used to describe the entire sample. For example, a single matrix A^q_T describing a coating with four interfaces is

$$A^q_T = A^q_1 A^q_2 A^q_3 A^q_4$$

Validation of Optical Codes also develops an expression for the transmittance of a thin film, which is sensitive to the whether or not the medium below the thin film is vacuum or bulk. This is the only project known to be using an expression that makes such a distinction, which is an issue that needs to be addressed when using silicon photodiodes as substrates. The transmittance of a beam with mixed polarization is

$$T = p_s \Re\left(\frac{k_{zs}}{k_{zv}}\right) |t^s_T|^2 + p_p \Re\left(\frac{n_v n^\star_s k_{zs}}{n_s n^\star_v k_{zv}}\right) |t^p_T|^2$$

where p_s and p_p are the fraction of s and p polarized light, and the operator $\Re()$ calls for the real part of the argument to be used. The subscripts s and v identify the material below the coating and the material above, respectively. The t^q_T terms express the total transmittance of s and p polarized light through the entire coating. Similar to the matrix A^q_T, the total transmittance t^q_T is a product of the transmittances at each interface. The transmittances of s and p polarized light through the ith interface is

$$t^s_i = \frac{2k_{z1}}{k_{z1} + k_{z2}}$$

$$t^p_i = \frac{2N_1 N_2 k_{z1}}{N^2_2 k_{z1} + N^2_1 k_{z2}}$$

where, as before, the subscripts 1 and 2 refer to the material above and below the interface.

The equations presented here illustrate the method used for calculating reflectance and transmission.

It should be noticed that each k_{zi} term that appears in these expressions is dependent upon the index of refraction of the ith layer, N_i. For a full presentation of the derivation of the equations for the reflectance and transmittance through a single interface, the scattering matrix A_i, and the total reflectance and transmittance of a multilayer coating, *Validation of Optics Codes* or similar optical text should be consulted.

7.2 Analysis of Reflection and Transmission Data for Coating Thickness

Using the software package *R*, calculations using the CXRO optical constants and various thicknesses were compared to the reflectance data. Figure 20 illustrates the uniqueness of the thickness to producing a calculation which qualitatively resembles the measured data. Each of the graphs in Figure 20 has a calculation (solid line) with an interference peak at 42 degrees, matching the peak at 42 degrees in the measured reflectance data at 11.4 nm (cirlces). The three graphs attempting to match the data each use the same optical constants from the CXRO database, but differ in the total film thickness used in the calculation (17 nm at the left, 26 nm in the center, and 35.5 nm at the right). However, the top and bottom graphs are examples of fringe mismatches, easily identified since they have the wrong number of peaks present in the angles less than 42 degrees.

Figure 20 showcases the interference pattern in the reflectance data, but it should be noted that the leftmost feature in the data is not actually part of the interference pattern. Though it appears to be yet another maxima of the pattern, it is actually part of the total external reflectance curve associated with thin film behavior at near-grazing angles. Figure 21 describes the shape of the total external reflectance curve, as well as showing the dependence the position of the shoulder of this curve has on wavelength.[1] As wavelength increases, the shoulder of the total external reflectance curve drifts to larger angles. Since the angle nearest grazing at which data is able to be collected is 10 degrees (see 5.1) this shoulder is not seen in the reflectance data at wavelengths less than 6.5 nm. The features found in the EUV reflectance data, then, are more accurately attributed to both the interference arising from reflections from multiple interfaces, as well as from the total external reflection of the scandium oxide coating (when considering near-grazing angles at wavelengths larger than 6.5 nm.)

The program used to make the calculations in R is fully able to accommodate for any physical attributes of the film. From the HRTEM and STEM imaging performed on the coated silicon wafer and the coated silicon photodiode, a great deal about the physical characteristics of the bilayer

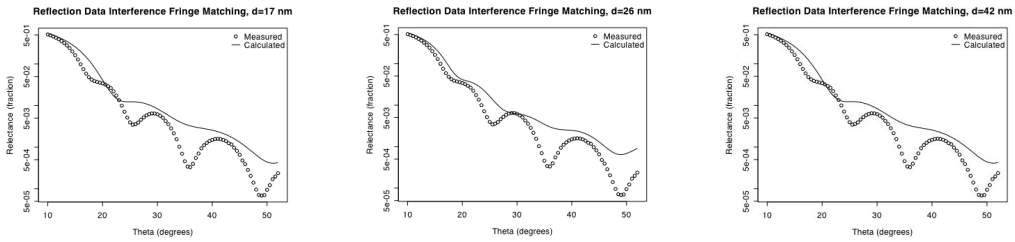

Figure 20: In the measurements of reflection versus angle, maxima and minima appear. These features are collectively referred to as the interference pattern. A single maxima is associated with a specific order. Proper matching of calculations to the observed interfernce pattern will only occur when the orders of the maxima match. In this figure, 11.4 nm reflectance data is shown compared to calculations done for three different film thicknesses: 17 nm at the left, 26 nm in the middle, and 35.5 nm at the right. The three graphs of this figure each show the maxima of the calculations lining up with the maximum of the measurement at 42 degrees. In the left and right graphs the film thickness' used in the calculations lead to an order mismatch, as evidenced by the incorrect number of maxima to among angles less than 42 degrees. This suggests that 26 nm is near the appropriate value for the thickness of the film, while 17 and 35.5 nm are incorrect film thicknesses.

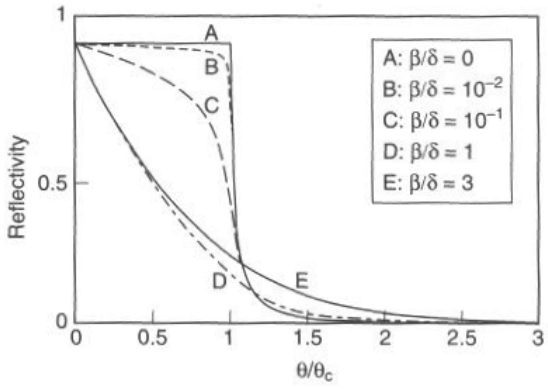

Figure 21: Depending upon the optical properties of the material, a thin film will have a critical angle (from grazing), θ_c, below which the film will exhibit total external reflection. The graph shown here (taken from Attwood) illustrates this with five curves, each with different $\frac{\beta}{\delta}$ ratios.

Sc0305 was learned, all of which was incorporated into the calculations made to model the data. As was found in the STEM images of Sc0305 Diode, the density ratio between the upper and lower layers was set so that the lower film of the bilayer was 90% as dense as the upper film. This means that in the model the scandium oxide must be described as a bilayer, where the optical constants of the lower part are coupled to those of the upper part by

$$n_l = (0.9 * n_u) + 0.1$$

$$k_l = 0.9 * k_u$$

Additionally, from the HRTEM and STEM imaging of Sc0305 Diode, values for the RMS roughness of the coating's surface and interior interfaces could be estimated. These were included into the calculation using Nevot-Croce correction factors using conservatively chosen values. The Nevot-Croce correction for the roughness of a specific interface is applied to the Frensel coefficient describing the reflection of that interface, and has this form:

$$e^{\frac{2\pi}{\lambda}\sqrt{N_1 N_2}\sigma_i^2}$$

where N_1 and N_2 are the complex indices of refraction above and below the interface, respectively, and σ_i is the root mean square roughness of the interface.[28, 29] In the sample studied, there are four interfaces in this coating. The silicon dioxide/silicon interface is taken to be nearly perfectly smooth, and not contributing to the calculation as far as roughness is concerned. The lower scandium oxide/silicon dioxide interface in the STEM images appears quite smooth as well, and it is assumed that the roughness it exhibits is similar to that measured on bare silicon wafers by AFM. The roughness value of this interface was chosen to be 0.4 nm. It is well known that thin film deposition almost always results in film surfaces with greater roughness than that of the surface they are deposited on. In the STEM images the upper scandium oxide/lower scandium oxide interface was in agreement with this principle and noticeably rougher than the lower scandium oxide/silicon dioxide interface. For this interface, between the layers of the bilayer, the roughness value was chosen to be 0.8 nm. Lastly, the surface of Sc0305 was considered, and a roughness value of 1.0 nm was chosen to describe its quality. This value was intentionally chosen conservatively, as the total roughness correction to the calculation will be dominated by the effects attributed to the vacuum/upper scan-

dium oxide interface. The STEM images of Sc0305 Diode suggest that the true roughness value for the coating surface was probably larger, as does previous experience with thin films of this type, but it was felt that underestimating the degree of roughness on the surface would be more reasonable for initial analysis. After preliminary results for film thickness had been found, the issue of identifying the most appropriate surface roughness for describing Sc0305 Diode would be revisited (described towards the end of this section).

In addition to establishing the density ratio of the films for the scandium oxide bilayer, the HRTEM images of Sc0305 Diode also provided the ratio of the thicknesses of the bilayer. The ratio between the thickness of lower layer and the upper layer is 1:9. The thickness of the lower scandium oxide layer is kept at 10% of the total bilayer thickness during the modeling of the measured data. During this modeling, the total thickness of the scandium oxide bilayer is varied to best match the calculation to the data.

Recall that even though the HRTEM images allow for the measurement of the total thickness of the bilayer and its components, the values for thickness taken from the images only provide a suggestion of the neighborhood of the true thickness of the film involved in the EUV measurements. With this in mind, the HRTEM measurements of Sc0305 Diode suggest the thickness of the total bilayer be in the neighborhood of 30-34 nm. The thickness of the silicon dioxide layer of the photodiode, however, should be uniform across the surface of the diode (unlike the deposited scandium oxide thin film). Measurements of the thickness of the silicon dioxide layer from the HRTEM images can be taken as *the* thickness of that layer. Since the silicon dioxide layer is amorphous, it is actually considerably easier to distinguish its boundaries in the images than crystalline films. Surprisingly, the thickness of the silicon dioxide layer consistently appeared in the HRTEM images to be 4.3-5 nm, despite assurances from IRD that the layer is 6-6.5 nm thick. Granted, in the measurements from the HRTEM images there is some judgment applied to defining where the silicon dioxide layer begins and ends. However, the error inherent to the values culled from the images is not on the order to place the thickness measured in the HRTEM in agreement with that coming from the manufacturer. On the other hand, if the silicon dioxide thickness provided by IRD is more accurately defined as the thickness of the actual silicon dioxide layer *plus* the thickness of the detector's dead layer, the HRTEM measurements are in harmony with the IRD values. The thickness of the silicon dioxide layer used in the modeling of the data is 4.8 nm.

By incorporating the results of the characterization of Sc0305 Diode to develop a physical description of the film, the modeling of EUV R&T data was set to begin. The model would describe the sample

Sc0305 as follows:

- The scandium oxide thin film coating is a bilayer.
- The lower layer of the bilayer is 90% as dense as the top.
- The lower layer constitutes 10% of the total thickness of the bilayer.
- The thickness of the silicon dioxide layer of the detector is 4.8 nm.
- The RMS roughness, in nm, of the interfaces of the sample is
  - 1 (vacuum/upper scandium oxide layer),
  - 0.8 (upper scandium oxide/lower scandium oxide layer)
  - 0.4 (lower scandium oxide/silicon dioxide layer)

To determine the thickness of Sc0305 Diode, R&T data was modeled in the 8.4-11.6 and 11.2-14 nm wavelength ranges. The data in these wavelength ranges was chosen for film thickness analysis over the other data collected because both the reflection and transmission data in these ranges exhibit the highest quality. Additionally, the angular range collected in the measurements of these wavelength ranges is quite large. Theta values for the 8.4-11.6 nm range cover 10-48.5 degrees, while the in the 11.2-14 nm range theta runs from 10-52 degrees. In both cases, this large theta range is enough to show several interference fringes in the reflection data: as many as five fringes are seen in the 8.4-11.6 nm data, and up to three are present in the 11.2-14 nm data. With the presence of the interference maxima and minima (of several orders) in the data, agreeable fits between calculation and measured data would strongly suggest the values resulting from such fits were indeed close to the true values of the parameters.

The routine followed to model the data was selected to have a specific order, which would focus on adjusting the parameter most likely the main contributor responsible for a majority of the error between the calculation and the measured data. To determine the thickness of Sc0305, the analysis of each R&T data file in the two selected wavelength ranges (32 data files in the 8.4-11.6 nm wavelength range, 28 data files in the 11.2-14 nm wavelength range) was done in this order:

1. Fit the optical constants n and k of the scandium oxide bilayer.
2. Fit the total scandium oxide bilayer thickness d.
3. Fit the optical constants n and k of the silicon dioxide layer.
4. Fit the total scandium oxide bilayer thickness d.
5. Fit the optical constant k of the scandium oxide bilayer.
6. Fit the optical constant n of the scandium oxide bilayer.
7. Fit the total scandium oxide bilayer thickness d.

Step 3 examines the optical properties of the silicon dioxide layer below the deposited scandium oxide thin films. Silicon dioxide is a very well studied material, and it was expected that the optical constants available through the CXRO database would be accurate in describing how it would behave in the EUV. However, it is not known whether or not the silicon dioxide present on the IRD photodiode is thermally grown or if it is deposited. As mentioned in Chapter 1, in the EUV the optical performance of a material has an increased sensitivity to practically all parameters. Most likely there are some subtle differences between the silicon dioxide present in Sc0305 Diode and the silicon dioxide from which the CXRO optical constants were generated. For this reason, it was decided that the fitting of the silicon dioxide n and k in step 3 was justifiable.

This fitting sequence is illustrated in Figures 22 thru 29.

The preceding description of the modeling sequence mentions the error calculation between the measured data and the generated curve. This error value is monitored by the program used for the simulation as the parameters allowed to vary are changed, until the error value is determined to be a minimum. Originally, this error calculation was simply a sum of the square of differences between the measured and generated values at each theta value. However, it was soon realized that achieving a good fit to the data was more involved than simply allowing the code to "minimize the gap" between the calculation and the measurement.

As the fit routine outlined above was being developed, a weighting scheme was introduced that would place emphasis on the low-angle data such that an error between the calculation and the measurement there would be much more significant than errors elsewhere between the patterns. A Gaussian distribution was used to determine the weighting parameter versus angle, centered about

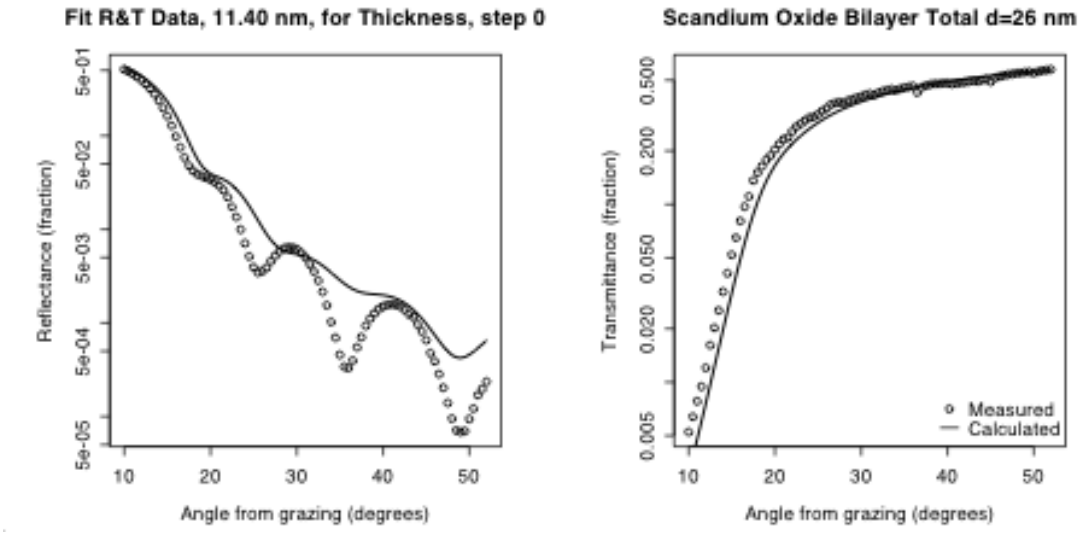

Figure 22: Measured reflectance and transmittance at 11.4 nm, and the calculation using CXRO optical constants are shown here. A thickness value for the film of 26 nm was used to begin modeling. Notice the calculated and measured maxima coincide at 42 degrees, and that the fringe order appears correct.

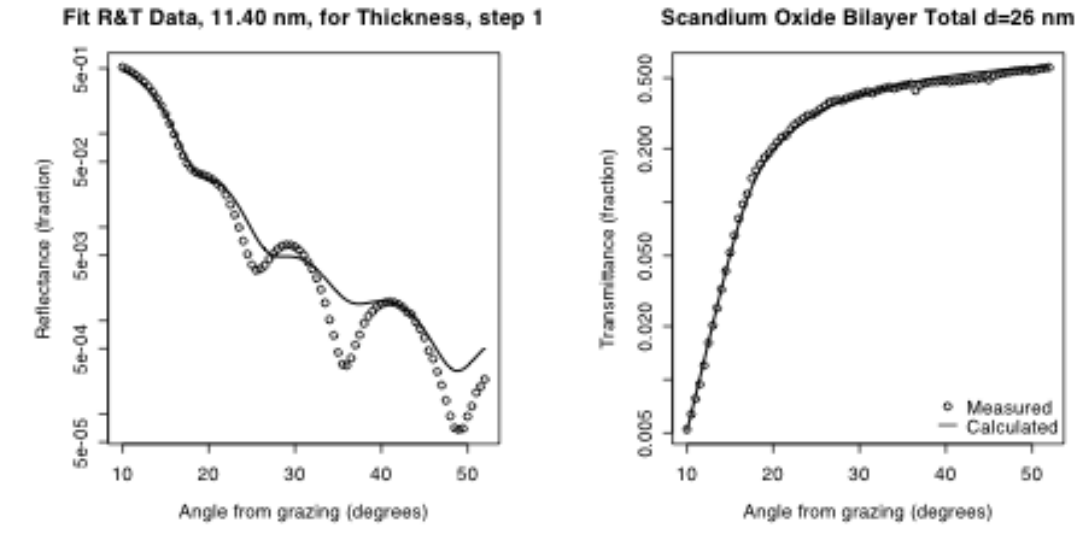

Figure 23: The data fitting sequence begins by varying the optical constants n and k of scandium oxide to find values which result in the best match between calculation and measurement.

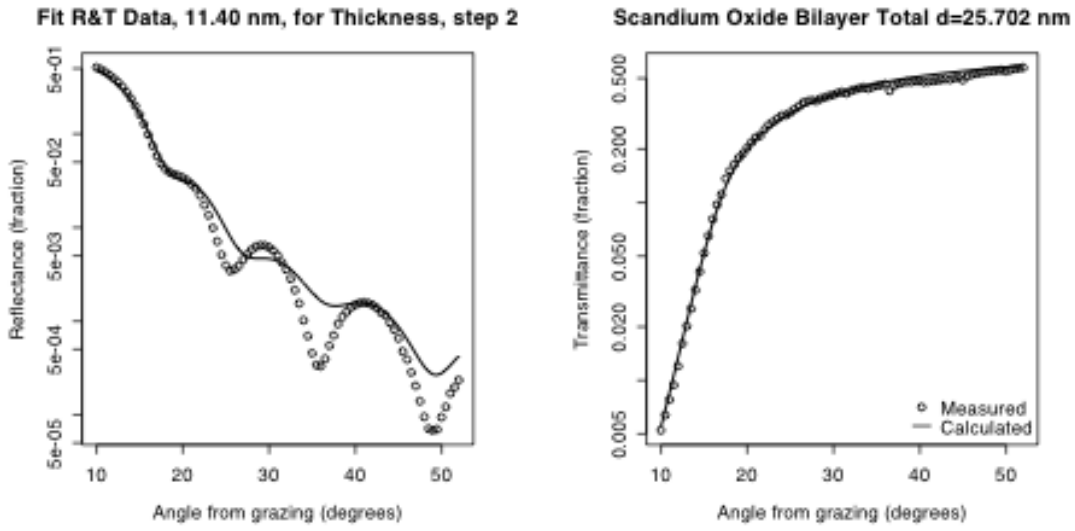

Figure 24: In the second step of the fitting sequece, the thickness of the scandium oxide thin film is allowed to vary. This essentially shifts the calculated pattern left or right to align the calculated maxima and minima with those of the measurement. The optimal total film thickness at this point is calculated to be 25.70 nm.

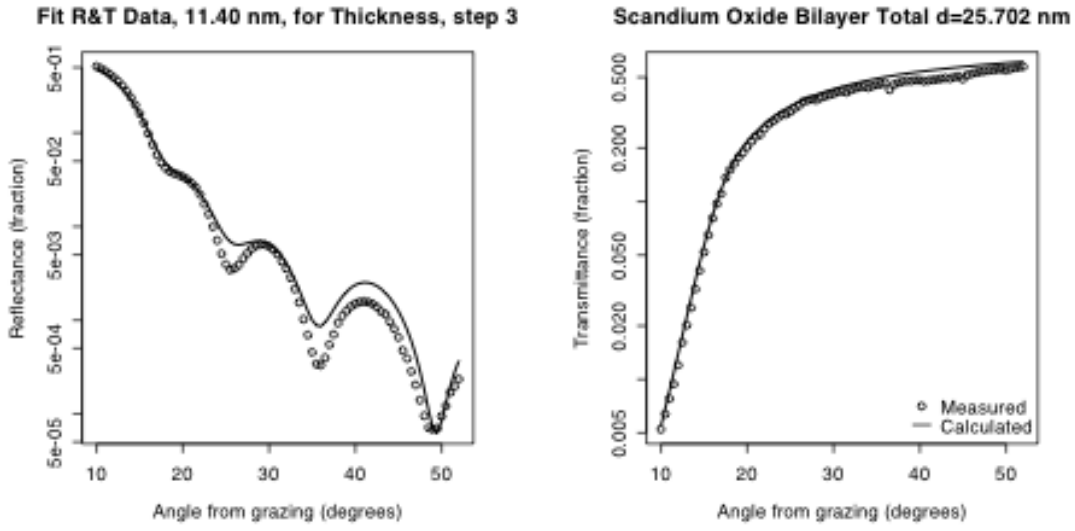

Figure 25: The optical constants of the silicon dioxide layer atop the silicon photodiode substrate are now allowed to vary (step 3 in the fitting sequence). This results in the depth between the maxima and minima of the calculation more closely resembling the measurement.

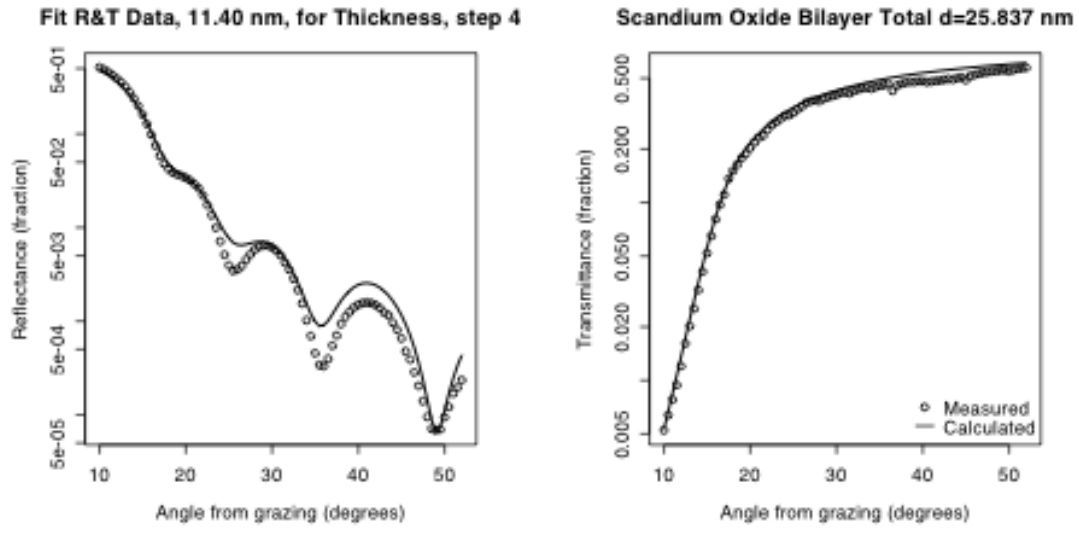

Figure 26: In step 4 of the fitting sequence, the thickness of the scandium oxide thin film is again allowed to fit. The resulting calculated thickness is only 0.1 nm (less than 0.5%) different that the value before this step was performed.

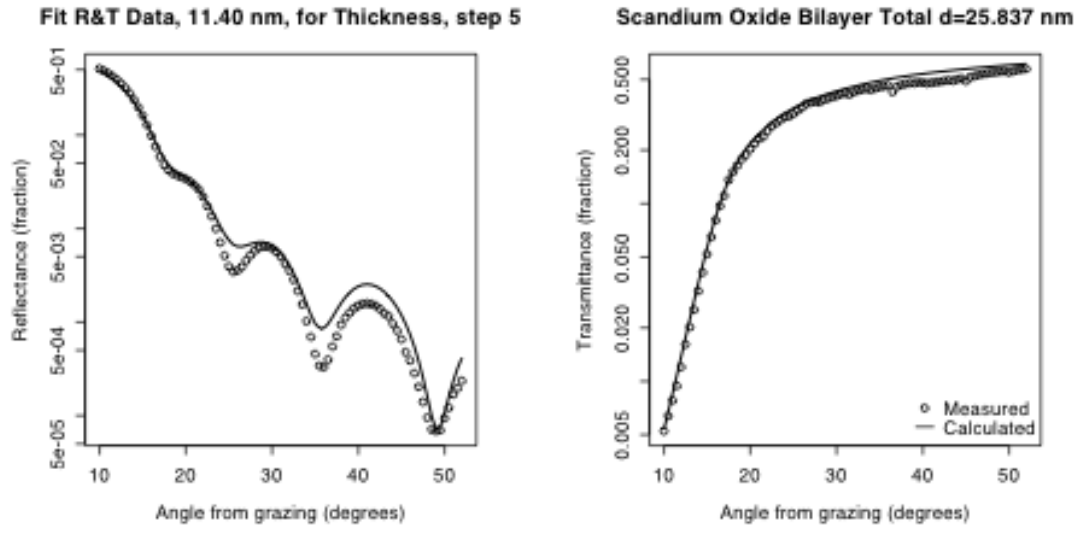

Figure 27: In step 5, the refractive index, n, of scandium oxide is allowed to fit. Variations of this parameter mostly change the calculated reflectance, though the calculated transmittance curve is also effected slightly.

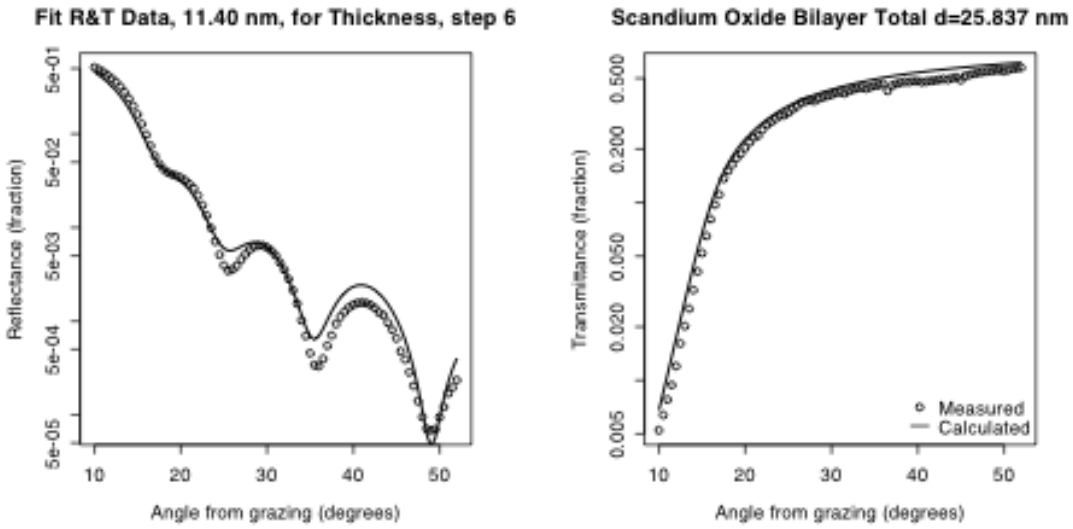

Figure 28: The absorption coefficient, k, of scandium oxide is allowed to fit. This variable has the most effect the the transmittance curve, and does not effect the calculated reflectance much at all.

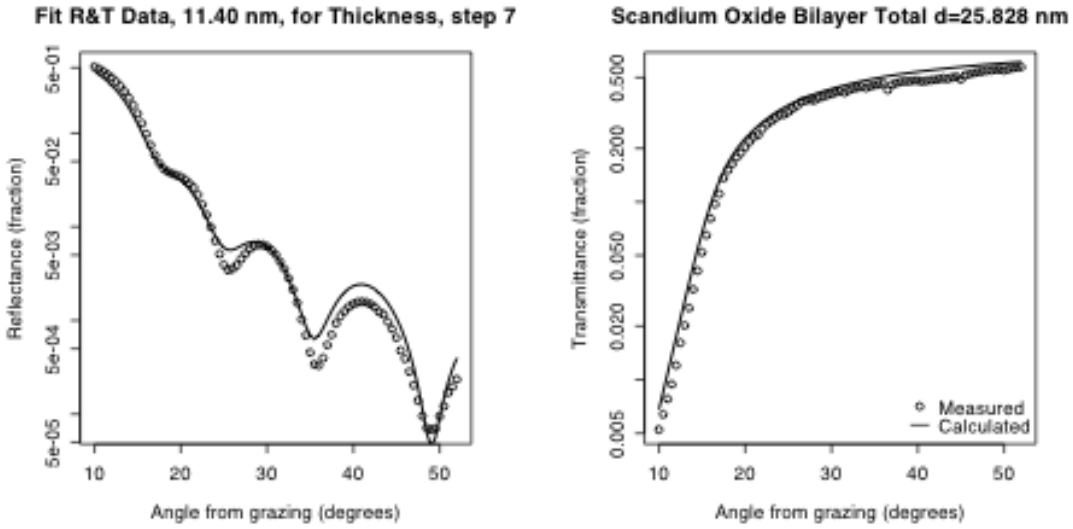

Figure 29: The final step in the fitting sequence it to allow the thickness of the scandium oxide to vary one last time. This is essentially to allow for a final adjustment to the positions of the maxima and minima, which may have shifted slightly in the adjustments to n and k earlier. The resulting value for the thickness of the scandium oxide thin film is again less than 0.1 nm different than the value before the fit was performed.

the lowest angle of the scan, 10 degrees. This implementation proved to increase the sensitivity of the algorithm to determining proper values for n_{i}, as n_{i} is the parameter which is most influential over this part of the pattern (which, in fact, in these parts of the wavelength range is the shoulder of the curve showing total external reflectance). Soon, though, it appeared that this low-angle weighting was leading to consistent mismatches between the calculated pattern and the measured data at the larger theta values. To resolve this, a second weighting scheme was introduced in addition to the use of the near-grazing Gaussian, though this time the weight was applied to the error between the *slopes* of the calculated and measured patterns. This would ensure the qualitative shape of the generated graph at larger angles was of greater importance there than the actual values. Away from grazing, the reflectance data is influenced by several factors. At larger angles, the complications from interface quality and interface/surface roughness become more and more apparent, while at the same time more and more difficult to quantify. After developing more insight into the subtleties of the interference pattern, a new approach to error weighting was developed. The new weighting scheme is given the name "adaptive weighting".

Adaptive weighting assigns the most significance in the error assessment to the portions of the measured data where the slope is the smallest, which is at the peaks and valleys of the interference pattern. This weighting is termed "adaptive" because the collective weighting values, which are called the slope signature, are generated from and specific to the individual reflection data set being considered (as illustrated in Figures 30 thru 33). The slope signature is determined by first numerically evaluating the slope of the normalized reflection data at each theta value.

$$m_i = \frac{r_{i+1} - r_{i-1}}{\theta_{i+1} - \theta_{i-1}}$$

The absolute value of the slope of the measured reflectance is then inverted, after which the natural log is taken. This value is cubed in a final step to accentuate the local maxima in the slope signature.

$$\varsigma_i = \left[\log\left(\frac{1}{|m_i|}\right)\right]^3$$

This expression is for a single element of the slope signature, ς. Figures 30 thru 33 illustrate the adaptive weighting concept by displaying measured reflectances at different wavelengths, and the slope signatures unique to that measurement. In each figure, it is easy to notice the differences in the interference pattern of the data as well as the differences in the slope signatures.

Each file of data in the two selected wavelength ranges was modeled as described in the preceding

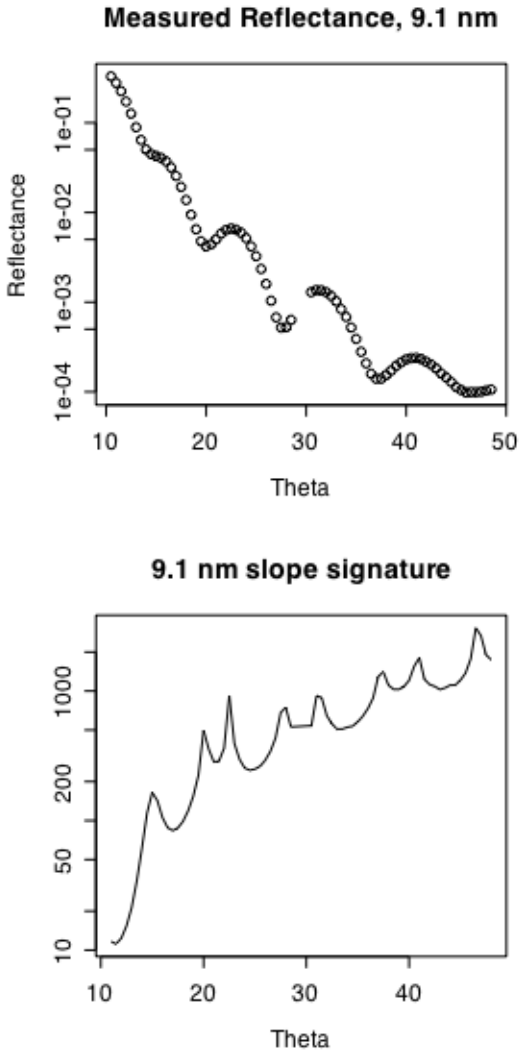

Figure 30: The top graph shows reflectance versus angle at 9.1 nm. The slope signature generated from the measured reflectance is shown in the lower graph.

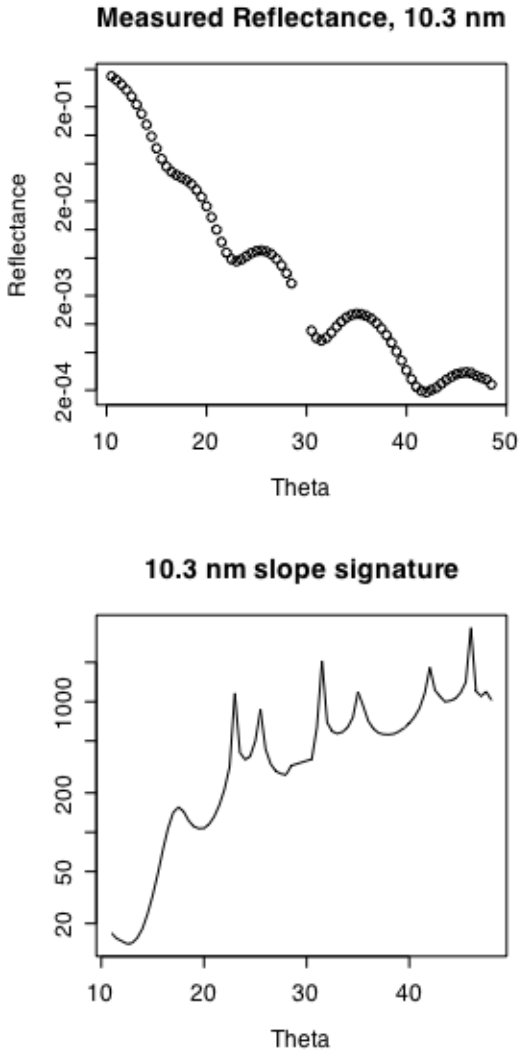

Figure 31: Again, the top graph shows measured reflectance, however here at 10.3 nm. The interference pattern seen in the data is noticeably different than that in 30. The slope signature characteristic of the 10.3 nm data is shown in the lower graph. Since the slope signatures are generated from the measured data, the are unique to that individual data set.

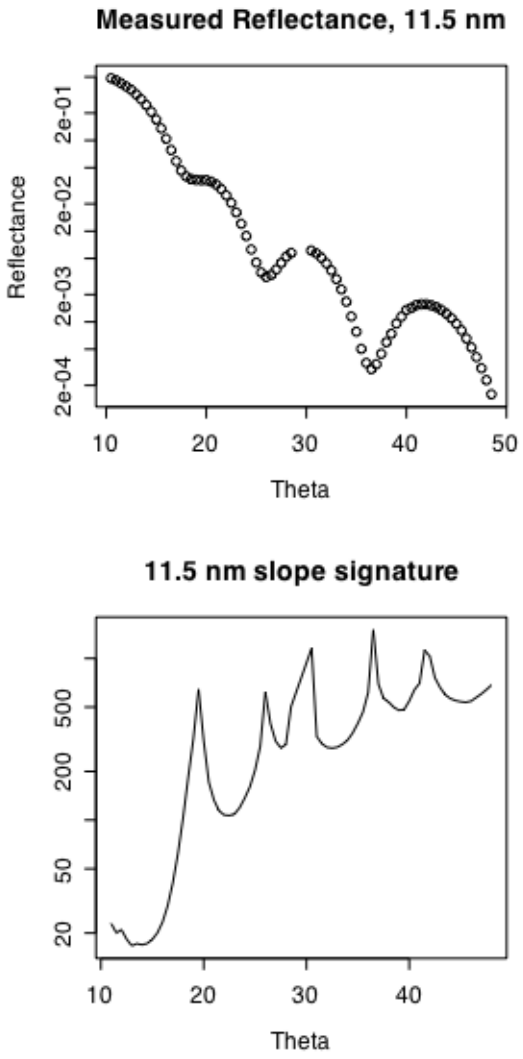

Figure 32: The slope signature concept is further illustrated by examining reflectance data at 11.5 nm. As before, there are differences apparent in the data was well as the slope signature.

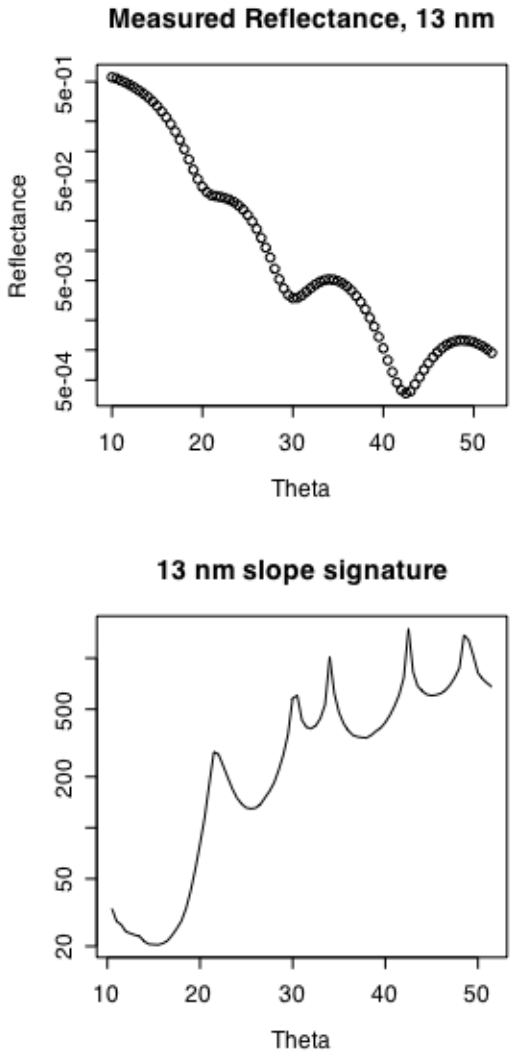

Figure 33: At longer wavelengths, the interfernce pattern has a greater separation between the neighboring maxima. The slope signature reflects this also. Comparison to the data and slope signature seen in Figure 30 again illustrates how the slope signature is adaptive to the data being studied.

paragraphs. In total, sixty sets of reflectance and transmission data were fit, and the results analyzed to determine the optimal thickness of the scandium oxide bilayer of Sc0305 Diode. The results of the analysis was a collection of bilayer thicknesses, with an average value of 28.91 nm, and a standard deviation of 0.25 nm.

When the values for the roughness of the interfaces were described earlier in the chapter, it was mentioned that the surface roughness of Sc0305 was in all likelihood greater than the 1.0 nm roughness being attributed to it in the model. To investigate this further, the value of the surface roughness was increased to 1.2 nm, and all sixty of the R&T data files previously modeled were analyzed again, following the same routine. The results from fitting with this modified surface roughness was slightly different than before: the average value for the the total thickness of the bilayer was 28.94 nm, with a standard deviation of 0.23 nm. It was intriguing that the standard deviation was lower when the sample description included a rougher surface. To investigate this further, the surface roughness was modified again and the analysis repeated. This was done for several surface roughness values, with the results presented in Table 3.

A minimum occurs among the standard deviation values when the surface of Sc0305 is described with 2 nm RMS roughness. However, upon examining the individual fits from the 2.0 nm analysis, the quality of the fits is actually poorer than those of the 1.8 and 1.9 analyses, despite having the lower standard deviation. After reviewing the family of fits from the analysis with 1.8, 1.9, and 2.0 nm surface roughness values, the most appropriate value for surface roughness was chosen to be 1.8 nm.

Having decided to use results found with this physical description, more scrutiny was placed upon the individual data fits from the analysis in which 1.8 nm was used as the surface roughness value. With increasing wavelength, the maxima of the interference pattern drift to larger theta values. Also, with longer wavelengths, the shoulder of the total external reflectance curve drifts to larger theta values, too. These two trends lead to this state: The reflection data at wavelengths longer than 13 nm apparently lacks sufficient features to be sensitive to variations in the thickness parameter during the modeling. Actually, the thickness values found from modeling this longer wavelength data are so different from the mean that they become key contributors to the standard deviation. For this reason, fit results from the analysis of R&T data collected between 13-14 nm was not considered to be as accurate as the fit results from analysis over 8.4-12.9 nm. The final determination of the thickness was found by using the results from modeling fifty data sets instead of the original sixty. From this, the total thickness of the scandium oxide coating was found to be 28.46 nm, with a

RMS Surface Roughness (nm)	Average Bilayer Thickness (nm)	Standard Deviation (nm)
1.0	28.91	0.2535
1.2	28.94	0.2332
1.4	28.99	0.2115
1.6	29.07	0.1900
1.8	29.55	0.1699
1.9	29.22	0.1601
2.0	29.27	0.1504
2.2	30.35	0.2118

Table 3: The results from fitting the reflection and transmission data in the 8.4-11.6 and 11.2-14 nm wavelength ranges, considering a variety of RMS values to describe the surface roughness. The original analysis of the data in the 8.4-11.6 and 11.2-14 nm wavelength ranges used an RMS roughness of 1.0 nm to describe the surface of the scandium oxide thin film, which was considered to be an underestimate. Data in the two wavelength ranges was analyzed again using an RMS roughness value of 1.2 nm for the surface, and it was noticed that the standard deviation decreased slightly. Again the data was refit with a larger roughness parameter, 1.4 nm, and the standard deviation decreased again. By gradually increasing the RMS roughness of the surface, an optimal value of 2.0 nm was found to correspond with the least standard deviation in the resulting film thicknesses.

standard deviation of 0.065 nm.

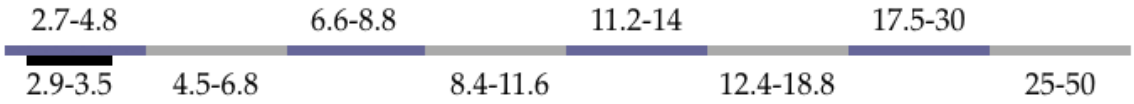

Figure 34: This bar represents the wavelength ranges, in nm, over which Sc0305Diode was measured. Each segment represents a different wavelength range. Notice there is some overlap among neighboring ranges.

8 Optical Constants of Scandium Oxide in the EUV

By analyzing the interference patterns which appear in the reflectance data over the wavelength ranges of 8.4-11.6 and 11.2-14 nm, the thickness of Sc0305 Diode was determined to be 28.46 nm. With this, the physical description of the scandium oxide thin film coating on the photodiode is complete.

Analysis of the R&T data in each of the wavelength ranges measured could now be performed to determine the optical constants n and k appropriate to the deposited film. Figure 34 shows the nine wavelength ranges over which Sc0305 Diode was measured. Notice that the wavelength ranges overlap slightly. This provides a convenient way to step from analyzing data in one wavelength range to analyzing data in another, which will be discussed in more detail later. Also, Figure 34 shows that at the short wavelength end of the measurements, there is a small wavelength range that is covered twice. Compared to the measurements made over 2.7-4.8 nm, the data collected in the 2.9-3.5 nm range was taken with twice the number of theta points (10-20 degrees, every 0.5 degree) and with a much finer wavelength step (every 0.02 nm) in order to fully examine the electronic transition features that scandium oxide exhibits around 3 nm.

This analysis was done following a routine similar to that employed earlier to determine film thickness. A sequence of fits would be developed that would find the optimal value for the parameter(s) believed to be contributing most to the error between the calculation and measured data. Admittedly, having one less parameter to vary (since the thickness of the scandium oxide bilayer has been established) proved this modeling to be much simpler than that done before. In general, the following routine for fitting the data was found to work best:

1. Fit the R&T data, varying the scandium oxide n and silicon dioxide n.
2. Fit the R&T data, varying the scandium oxide k and silicon dioxide k.
3. Fit the R&T data, varying the scandium oxide n and silicon dioxide n.
4. Fit the R&T data, varying the scandium oxide k and silicon dioxide k.

The quality of the fit was judged using the sum of the differences between the calculated and measured reflectance and transmittance at each wavelength. For the analysis of the optical constants, there was no weighting employed in the determination of this error, in contrast to the process developed for analyzing data to determine film thickness.

Recall that in the previous modeling to determine the thickness of Sc0305 Diode, the indices of refraction n and absorption coefficients k of both the scandium oxide and silicon dioxide thin films were fit parameters. Rather than begin the analysis for the optical constants of scandium oxide by referencing the CXRO database, the n's and k's resulting from the thickness analysis were used as "seed" values to begin the analysis of the data, starting with the data collected at the wavelength 11.2 nm.

The modeling of the measured data to determine the optical constants was done one wavelength at a time, as before, using the R software and matrix-multiplication method. Upon the completion of modeling data at one wavelength, the program would import the reflection and transmission data for the next wavelength of the wavelength range. This new data would first be examined using the n and k generated results from the previous set as the seed from which to optimize the new n and k. Since the index of refraction and absorption coefficient for a material change smoothly versus wavelength (except at absorption edges), the seed values used to begin the analysis of each new data set should resemble the actual values. This minimizes the chance of the modeling code wandering into a different, inappropriate local minimum of the error surface.

Analysis of the reflection and transmission data in the nine wavelength ranges began by fitting the data at 11.2 nm, followed by the longer wavelengths of the 11.2-14 nm wavelength range. The neighboring wavelength range of 12.4-18.8 nm was then analyzed, taking the values for n and k of scandium oxide and silicon dioxide found when fitting the 12.4 nm data in the previous wavelength range as the seed. This process is illustrated in Figure 35. As mentioned at the beginning of the chapter, the overlap of the wavelength ranges allows for an easy transition to be made among the wavelength ranges in which data has already been analyzed to wavelength ranges yet to be modeled.

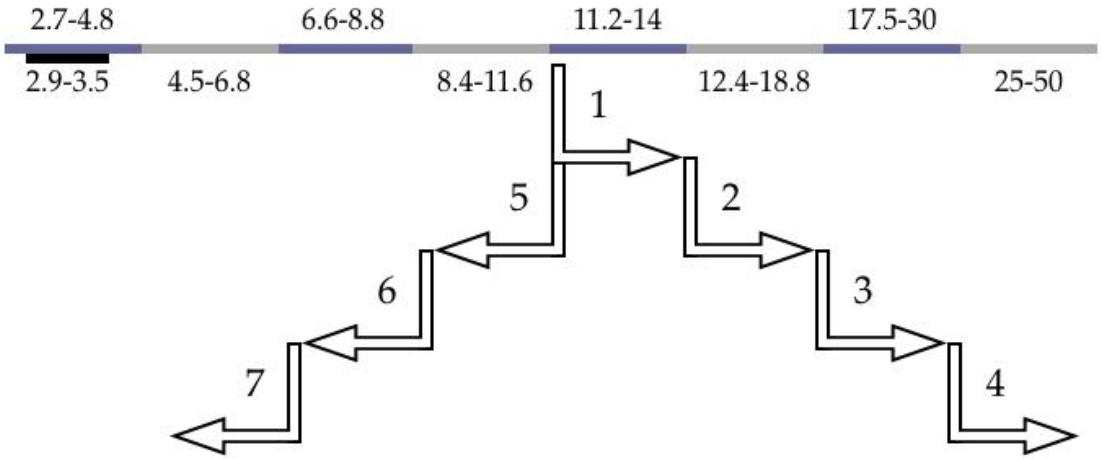

Figure 35: When fitting the reflection and transmission data from Sc0305 Diode to determine the optical constants of scandium oxide, the analysis was performed one wavelength range at a time. Beginning with the 11.2-14 nm wavelength range, the data was modeled. This diagram shows the sequence in which the reflection and transmission data from Sc0305 Diode was analyzed.

Figure 36 shows the optical constants n and k found for the scandium oxide coating of Sc0305 from 4.5-30 nm. For comparison, the optical constants available through the CXRO website are also included in the graphs as a solid line.

Figure 37 shows the results of the analysis of three data sets which cover 4.5-11.6 nm. Here it is seen that the collection of resulting n and k do not form a smooth curve as they should. The values of n and k which challenge the trend are likely incorrect, and appear on the short wavelength side of a data set. This portion of the data set is of lower quality due to a lower signal to noise ratio, and the resulting erroneous optical constants can likely be attributed to this. The incorrect values for n and k are unacceptable, and are removed from the collection of measured optical constants.

Figure 38 shows the optical constants, minus the offending values, over the wavelength range 4.5-11.6 nm, while Figure 39 shows the measured optical constants over the 11.2-30 nm wavelength range. Having allowed the optical constants of silicon dioxide to vary as a fit parameter in the analysis, it is also worthwhile to compare the values generated for n and k describing the layer of silicon dioxide to the tabulated values found at the CXRO website, shown in Figure 40.

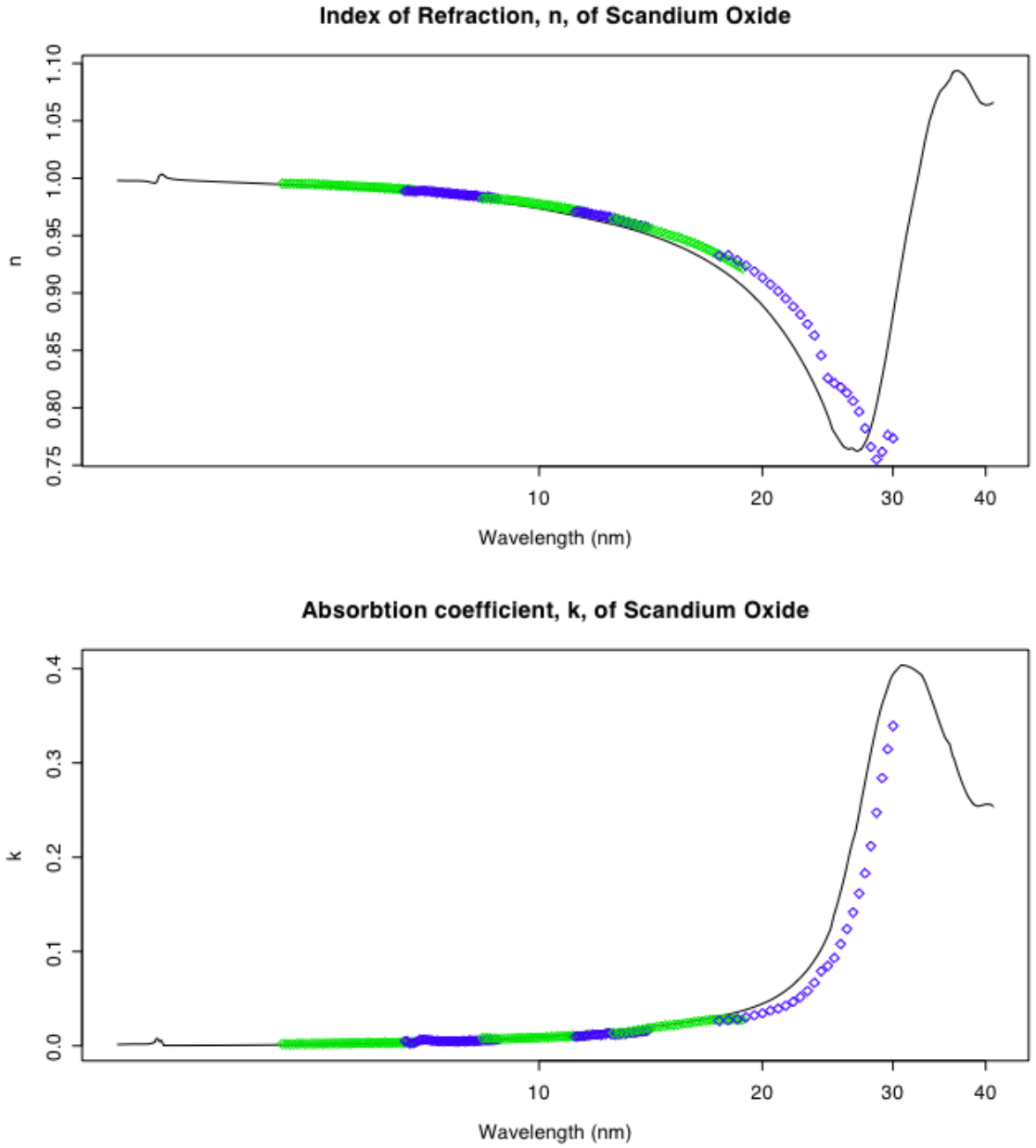

Figure 36: The experimentally determined optical constants for the scandium oxide thin film coating of Sc0305 Diode are shown in these two graphs. For comparison, the optical constants from the CXRO website are ploted as a solid line. Optical constants resulting from the of modeling the reflection and transmission data in six wavelength ranges are shown here. From the left, n and k for 4.5-6.8 nm are shown in light grey, 6.6-8.8 nm in dark grey, 8.4-11.6 nm in light grey, 11.2-14 nm in dark grey, 12.4-18.8 nm in light grey, and 27.5-30 nm in dark grey.

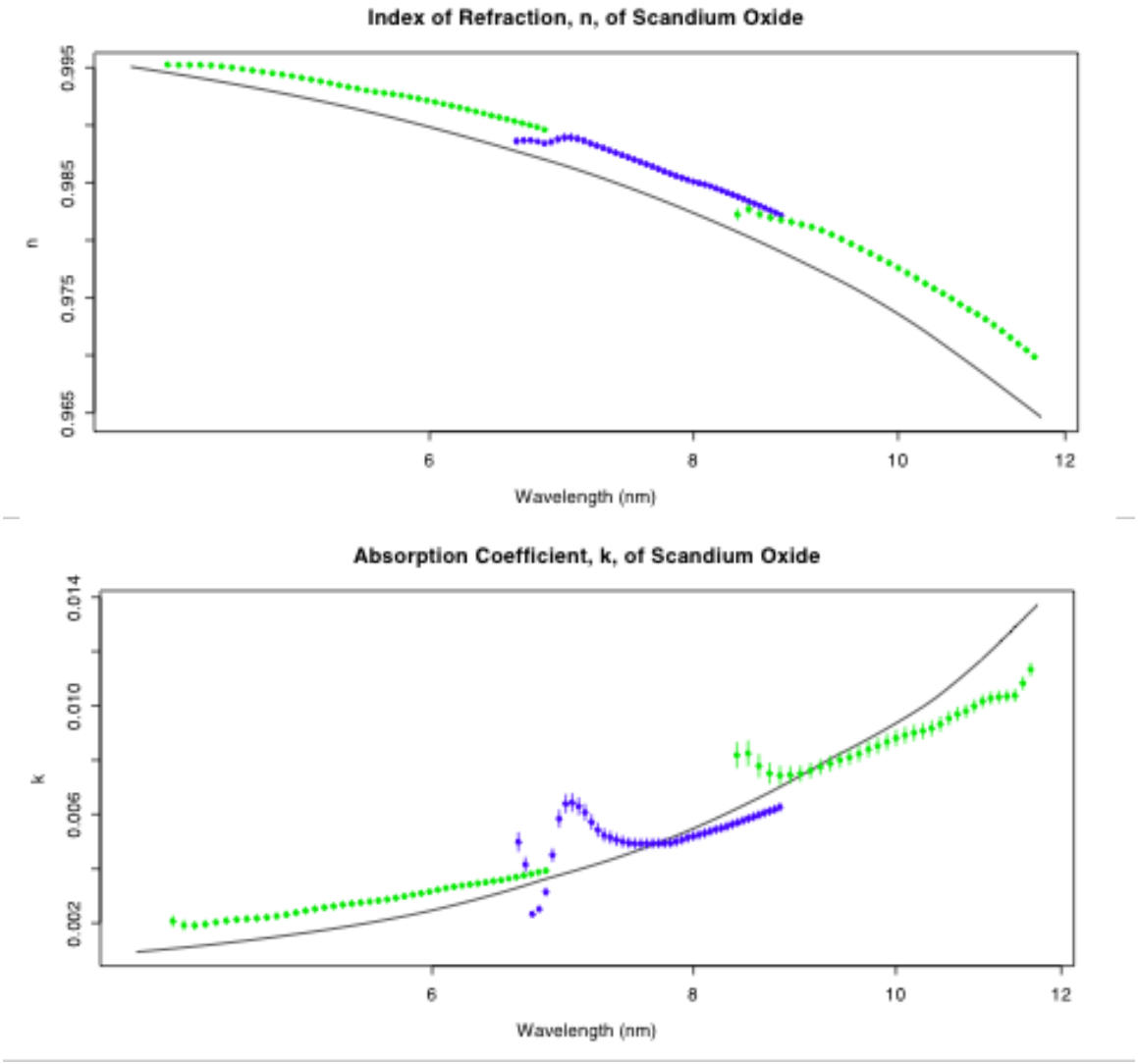

Figure 37: The experimentally determined optical constants of scandium oxide are shown from 4.5-11.6 nm. Again, the values for n and k for 4.5-6.8 nm are shown in light grey, 6.6-8.8 nm in dark grey, 8.4-11.6 nm in light grey, and the CXRO values plotted as a solid line. On this scale, it can be seen that towards the shorter wavelengths of each individual wavelength range, the results of the analysis are likely incorrect, though the trend established by the rest of the wavelength range seems acceptable. The incorrect values of n and k at the short wavelength end of the wavelength range may be due to the signal to noise ratio of the measurements becoming worse there. This issue may be resolved by modifying the analysis code to constrain the range of the fit parameters.

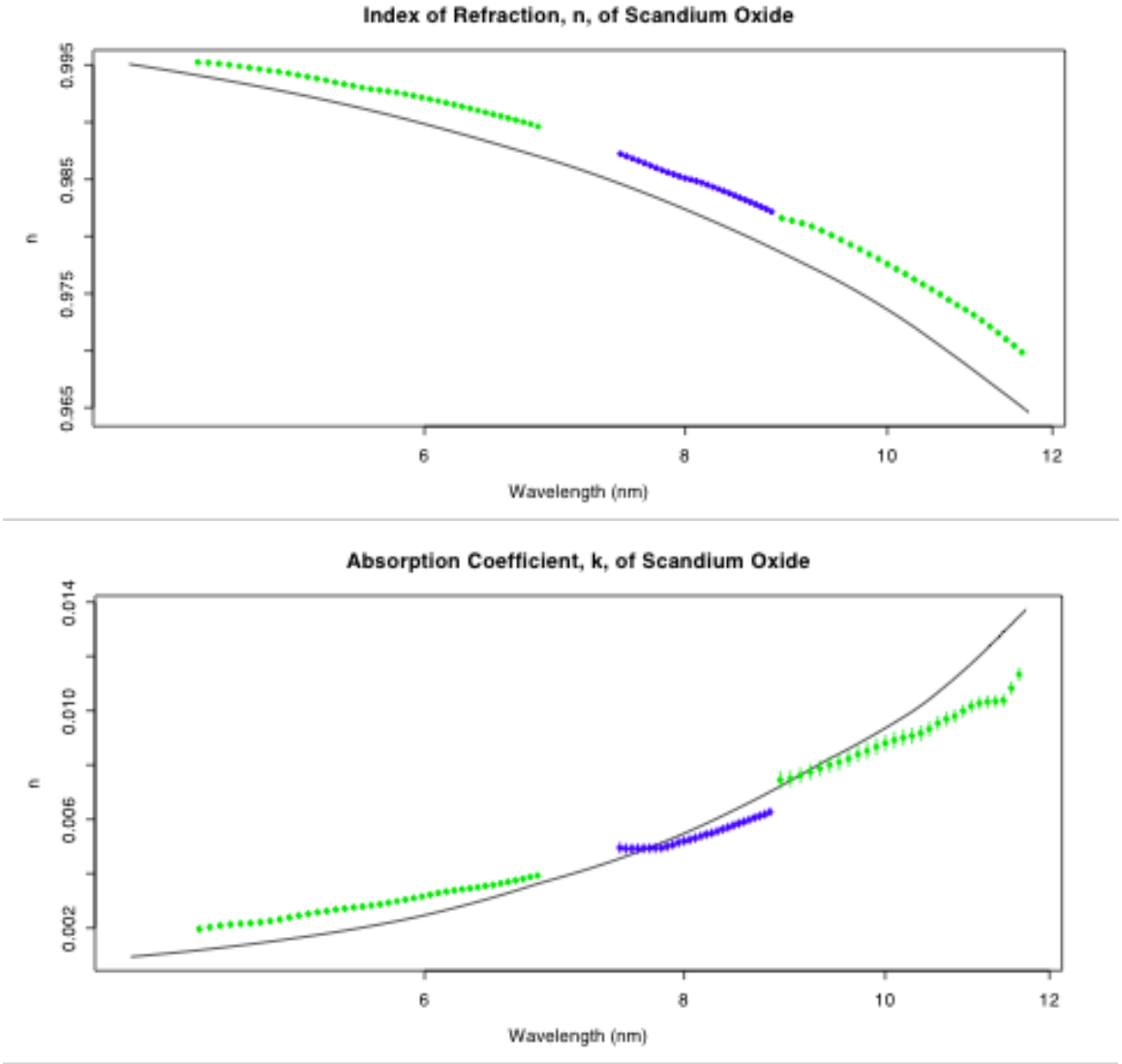

Figure 38: The experimentally determined optical constants of scandium oxide over 4.5-11.6 nm, with offending values removed. From the 4.4-6.8 nm data set, 3 data points were removed; 17 data points were removed from the 6.6-8.8 nm data set; and 5 data points were removed from the 8.4-11.6 nm data set. The solid line represents the values for n and k from the CXRO database.

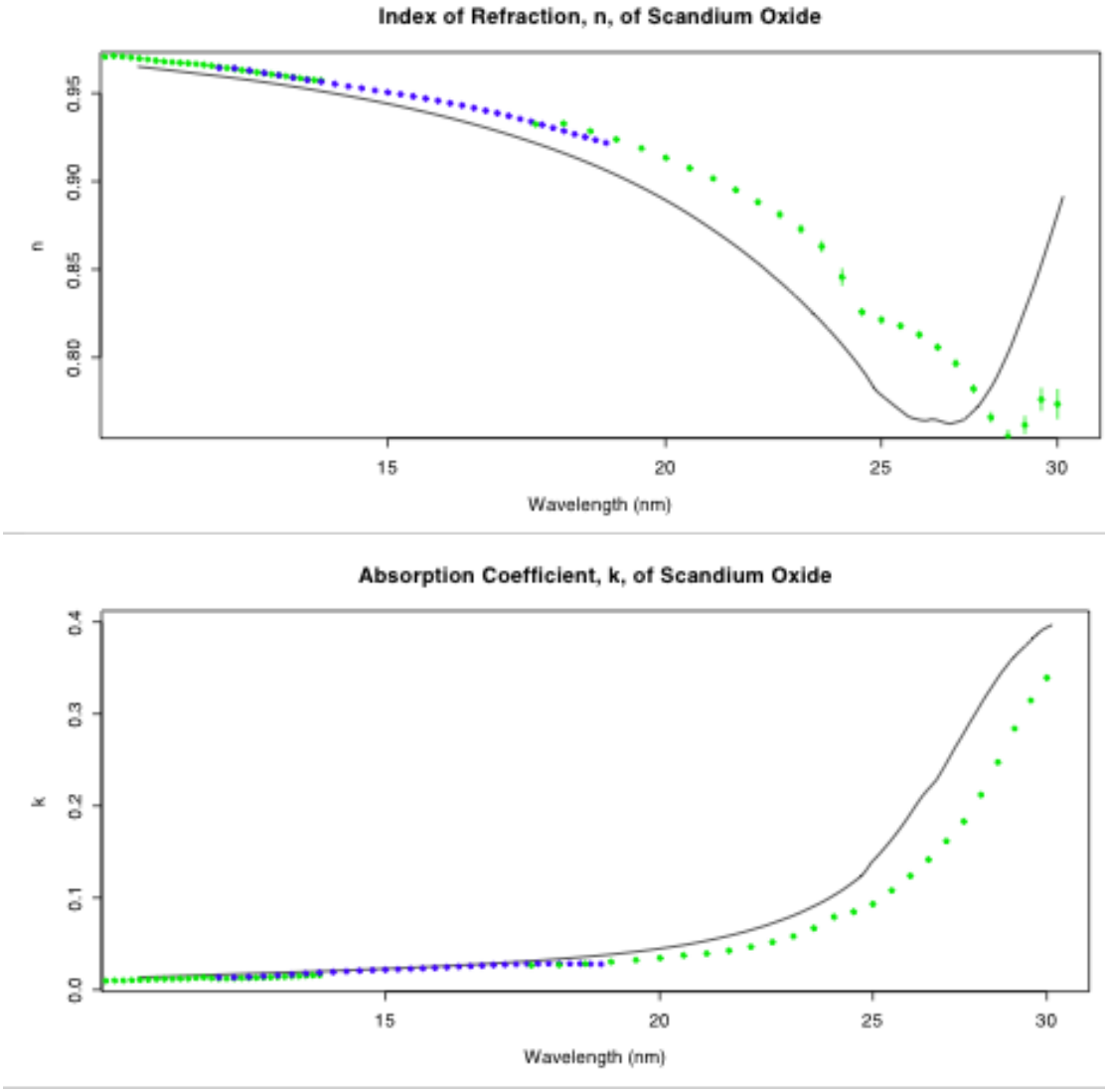

Figure 39: The experimentally determined optical constants of scandium oxide are shown from 11.2-30 nm. Values for n and k in the 11.2-14 nm wavelength range are shown in dark grey, 12.4-18.8 nm range are shown in light grey, and those for the 17.5-30 nm range are shown in dark grey. The solid line shows the values available from the CXRO database. Here, there is better agreement among the values of n and k from the different wavelength ranges than is found in the wavelength ranges represented in Figure 37. It is unclear whether or not the oscillation of values for n between 20 and 30 nm is physical or due to an inadequacy in the modeling process.

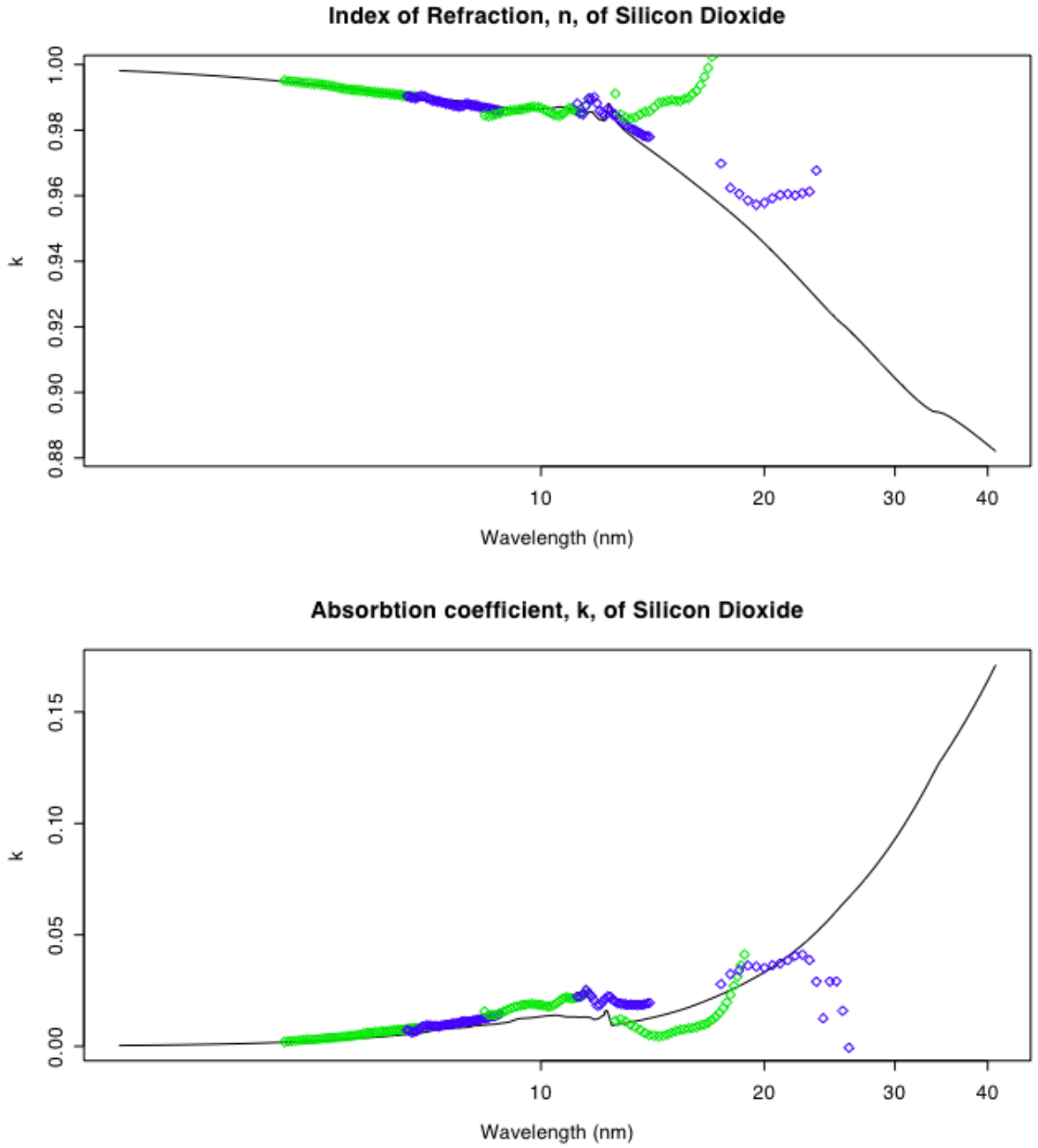

Figure 40: In the analysis of the reflection and transmission data from Sc0305 Diode, the optical constants of silicon dioxide at the surface of the diode were allowed to vary as a fit parameter. In general, the computed values follow the trend of the CXRO tabulated values (represented by the solid line), although there are notable discrepancies. Since the silicon dioxide layer is thin, though, its contribution to the accuracy of the calculation is small, and these agreements and discrepancies do not merit much attention. As with Figure 36, the n and k in the wavelength range of 4.5-6.8 nm are shown in light grey, 6.6-8.8 nm in dark grey, 8.4-11.6 nm in light grey, 11.2-14 nm in dark grey, 12.4-18.8 nm in light grey, and 27.5-30 nm in dark grey.

8.1 Imperfect Data in Portions of the EUV Range

When selecting the two wavelength ranges for the data used to determine the thickness of the coating on Sc0305 Diode (Chapter 7), the quality of the all the collected data was considered and wavelength ranges 8.4-11.6 and 11.2-14 nm were chosen to have the best data. To find the optical constants from the R&T data, however, in each of the wavelength ranges, there only exists one set of measured data. Regardless of quality, this data was analyzed, as there is no alternative.

In general, the reflection data over all the wavelengths measured is of high-quality, in which the data points collectively form a smooth, continuous curve. The reflection data begins to suffer from a low signal-to-noise ratio at the shorter wavelengths, where the reflected signal is extremely small and the gains of the preamplifiers must be set to maximum. This is particularly an issue with the reflection measurements made in the wavelength ranges 2.4-4.8 and 2.9-3.5 nm. With such markedly small reflection signals, it is not unusual for the reflectance in these ranges to be on the order of 10^{-3} near grazing, falling to 10^{-5} or 10^{-6} with increasing sample angle. Despite such low signals, though, the data still exhibited the easily discernible features of the interference pattern, though at angles beyond about 14 degrees the reflectance curve would become less smooth.

The quality of the transmission data over the entire 2.4-50 nm wavelength range can be summarized as excellent at longer wavelengths, but progressively poorer as wavelength decreases. At longer wavelengths, the transmission data is of high-quality, where the transmittance curve from the collective data points is quite smooth. However, in transmittance curves from shorter and shorter wavelengths, features appear in the curve that are discontinuities (several transmittance curves are shown in Figure 41). Originally, it was thought that these "drops" were possibly part of the true signal, though after becoming more familiar with the data through subsequent modeling sessions, this hypothesis was dismissed as unphysical. The features in question likely arise from problems in the data collection. As evidence of this, an inspection of the transmittance curves within a selected wavelength range shows that the suspect features do not exhibit any wavelength dependence, but instead appear at the same theta value with relative consistency. This is illustrated in Figure 42.

Additionally, a problem with transmission data at short wavelengths was noted. This, too, can probably be traced to the data collection. It was noticed that the transmittance curves very gradually decay in overall magnitude with shorter wavelength. This issue came to light because the calculated transmittance consistently appeared too high when analyzing shorter wavelength data. The error between modeled and measured transmittance tends to grow among shorter wavelengths within

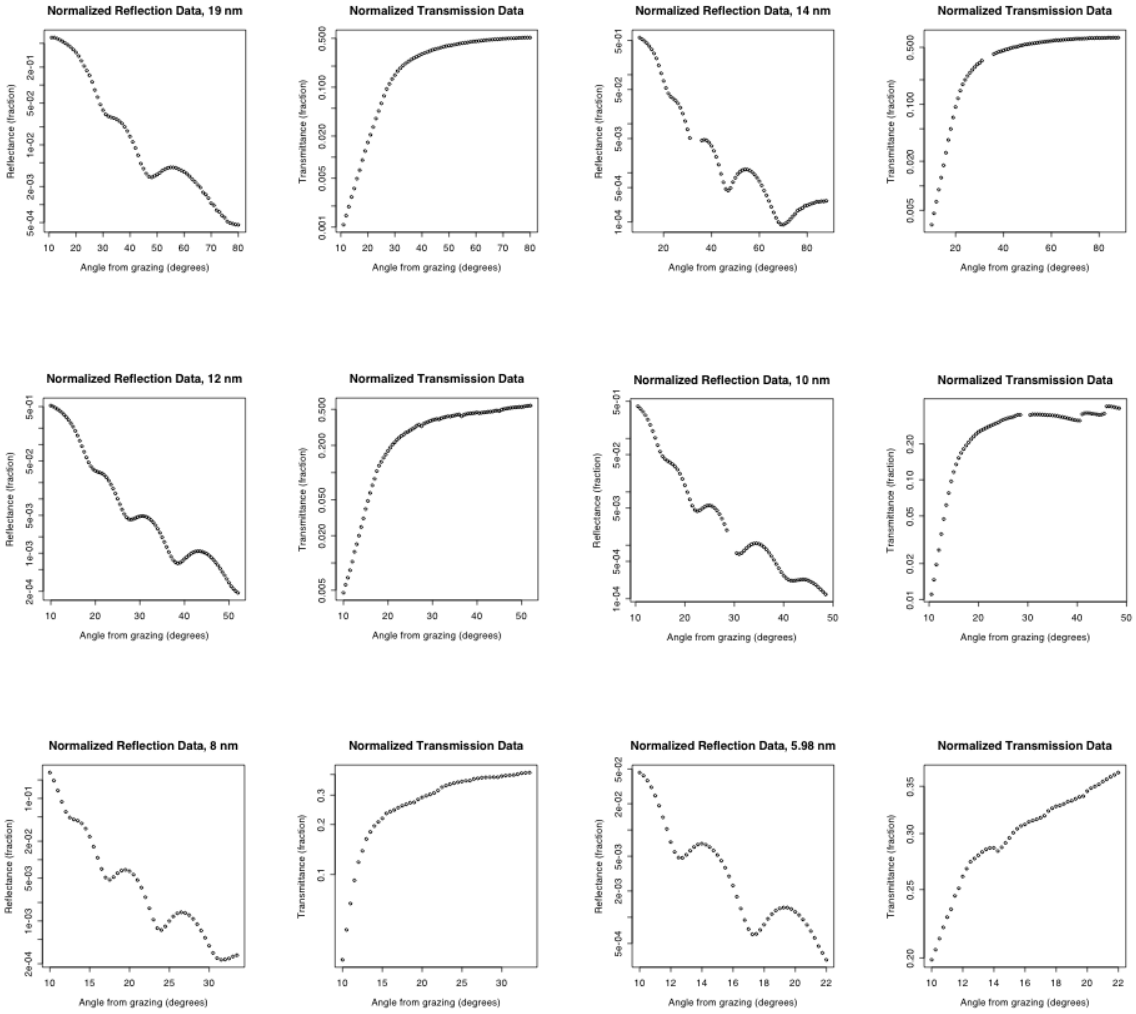

Figure 41: A sampling of normalized data from throughout the EUV range is shown here. The data graphs are arranged from longest to shortest from the top of the page down, from left to right. Each R&T data set is from a different wavelength range. In particular, the quality of the data can be gauged by the smoothness of the transmission curves. Overall, the data was of higher quality at longer wavelengths, while discontinuites appeared in the transmittance data more frequently and with greater prominence at shorter wavelengths.

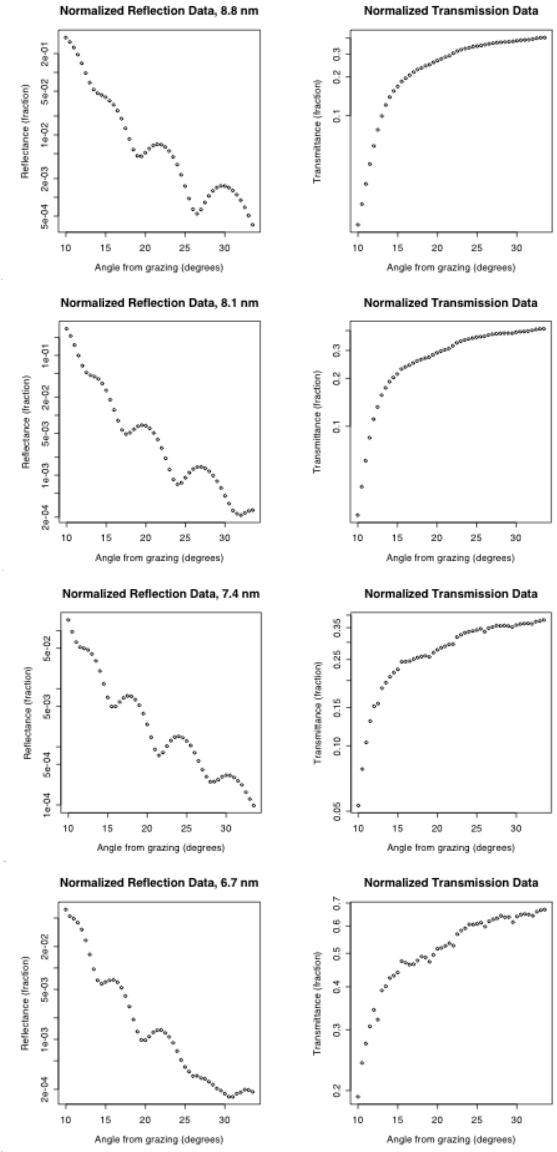

Figure 42: Data quality can vary within a wavelength range, as shown here. The R&T data presented in the four sets of graphs are all from the same wavelength range (6.6-8.8 nm). Notice the transmittance curve is smooth at the longer wavelengths, but becomes choppy as wavelength decreases.

a data set. This error was first attributed to incorrect calculations, due to incorrect absorption coefficient values describing the sample. It was believed that the seed values being used to begin each fit had drifted far enough from the true values for either n or k, or both, such that the fitting program had wandered into a different local minimum of the error surface. However, it was not possible to correct the calculated transmittance by adjusting either the k of scandium oxide or the k of silicon dioxide and maintain any harmony in the corresponding calculated reflectance. In particular, a substantial amount of time was spent trying various means and exploring different ideas that would hopefully produce calculations that were in better agreement with both the reflection and transmission data in the ranges 2.9-3.5, 4.5-6.8, and 6.6-8.8 nm. Only after investing considerable time and effort in trying to resolve this issue, was it concluded that most likely the fault lies somehow in the transmission data. There is the possibility that there is a unique combination of physical parameters and judiciously chosen optical constants that will remedy this problem, though at this point the data itself appears to be the culprit.

It is should be noted that this simultaneous reflection and transmission measurement technique using EUV light at the ALS is only recently developed and that its full use still being explored. Most likely, with more time spent using the technique and analyzing the resulting data, a proper explanation or solution to the low-quality transmission data at shorter wavelengths will be found. At this point, though, little could be done to accommodate for the realities of the data collected. The optical constants resulting from the analysis have a lower confidence limit because of this, though every effort was made to reproduce the measurements with the calculations. As a small consolation, inspection of the graphs of the resulting fits show that the reflectance data from 4.4-30 nm is fit very adequate. Though the reflectance curves are not particularly sensitive to the absorption coefficients, the graphs produced can only resemble the measured data as closely as they do if the generated values for k are in, at least, the vicinity of the actual values of k.

8.2 Unreliable Data from 25-50 nm

The optical constants generated from the analysis of the measured data fail to cover the 30-50 nm wavelength range, even though Sc0305 Diode was measured there. Indeed, analysis was attempted, but a problem was noted in the 25-30 nm range that showed the inadequacy of data collected using the magnesium filter over the 25-50 nm wavelength range. Prior to analyzing the data in the 25-50 nm range, the results of the analysis in the neighboring range, 17.5-30 nm, were consulted for seed values of n and k. The data in the 17.5-30 nm range was collected using an aluminum filter. It was

noticed that in the overlapping wavelength range the magnitudes of the reflectances, and to some extent the transmittances, are markedly different between the data collected with the magnesium filter and that collected with the aluminum filter. The magnitudes of the measured reflectances from each data collection should match (at the same wavelength) regardless of which filter was used. This is shown in Figure 43 with the 27 nm data. Most likely, this is due to the presence of higher-order light (photons with energies that are integer multiples of the desired photon energy) in the incident photon beam. The synchrotron light source is broadband source, so the energies of photons in the original, undiluted beam (before photon selection is done) cover a broad range. A diffraction grating monochromator to is used to separate the light by energy. The resulting beam is not monochromatic, but is instead composed of photons whose energies form a discrete set. The energies of this set include the desired photon energy, and energies which are integer multiples of the desired energy.

This situation is usually addressed by using a three-bounce-mirror to suppress the higher-order photons (this mirror filters out the photons above the energy of interest) and ultimately produce a monochromatic beam. The longer wavelengths of the EUV range available at the ALS, though, have only recently become available, and the optimal settings for the filter used in this range had not yet been developed when these measurements were made. With the disagreement in the magnitudes of the measured data between the two wavelength ranges, it was decided that analysis of the data collected from 25-50 nm would result in unreliable optical constants. This data was not modeled.

8.3 Sc0305 Diode from 2.9-3.5 nm

Earlier in the chapter, the shortcomings of the reflectance data were noted, in particular in the wavelength range of 2.9-3.5 nm. As mentioned, the reflectance from Sc0305 Diode in this wavelength range is very, very small. With the reflection signal so small, dark current becomes a more significant issue, especially when the value of the reflection signal is on the order of the dark current.

Coincidentally, this energy range contains the wavelengths associated with the L_2 and L_3 transitions of scandium. The presence of the transition at this wavelengths leads to a resonance in the index of refraction of scandium oxide. In this neighborhood, the optical constants n and k vary dramatically, complicating the analysis since at each wavelength the true values for n and k can be considerably different than the seed values taken from neighboring data sets. This increases the likelihood of the model drifting into the wrong portion of the error surface, and subsequently providing incorrect

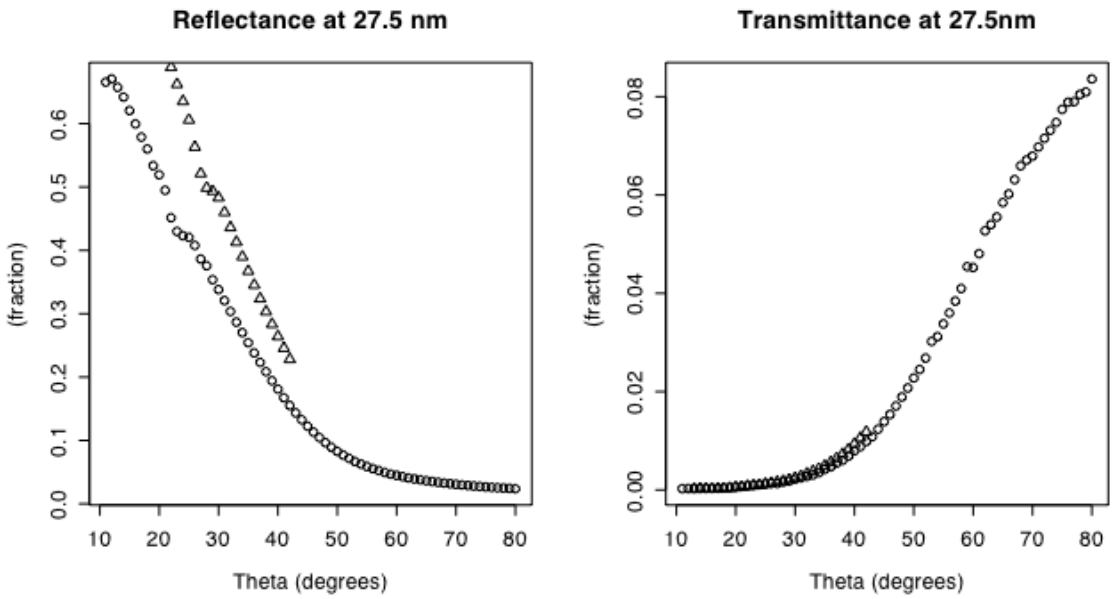

Figure 43: In the reflectance graph, two sets of data are shown. The data represented by the open circles is data collected at 27 nm with the ALS instruments set to access light in the 17.5-30 nm wavelength range. The data represented by the open triangles is also data collected at 27 nm, however this data was collected with the ALS instrument's parameters set to access light in the 25-50 nm wavelength range. At near-grazing angles there is a dramatic disagreement between the reflectance values. Ideally, the values of the reflectance would be the same since the coating being measured would respond identically to 27 nm light regardless of the arrangement used to access the light. The larger reflectance values are attributed to higher-order photons being present in the beam. Notice also that a trend is also noticeable in the transmission data that at angles farther from grazing the transmittance shown by the open triangles would be considerably greater than that shown by the open circles.

results.

Original attempts to model this data did exactly that. The model would generate values for n and k that were unphysical. As the code would scroll through the data for different wavelengths, a critical point would be encountered at which the estimation for the appropriate n's and k's would teeter into the wrong "territory" and the results from the subsequent calculations would be most definitely wrong.

It was noticed that on either end of this wavelength range, that the reflectance were quite small. However, the data three wavelengths inside the wavelength range had more acceptable values for the reflectance. Rather than model the data of this wavelength range in its entirety from one end to another, the wavelength range was split, and analysis was performed from 2.9-3.06 nm and 3.06-3.5 nm. To establish the values for n and k of scandium oxide and silicon dioxide with which to begin the modeling, the data at 3.06 nm was modeled manually. R was used to minutely change the index of refraction of scandium oxide until an optimal value was found, followed by a similar controlled monitoring of the calculations as the index of refraction was slowly changed. This process was repeated to find reasonable absorption coefficients for scandium oxide and silicon oxide, as well. Values were found for the n's and k's that provided a good match to the data at 3.06 nm, and automated analysis was begun. However, it was again found that the code could not successfully complete the analysis of the modified wavelength range, despite several different fitting schemes attempted.

In this wavelength range, the physical description of the film may be inadequate to enable proper analysis of the reflection data to be performed. At such small wavelengths, roughness becomes an even more important issue, and this may be a region where the Nevot-Croce correction for roughness is not sufficient or applicable.

8.4 Positions of Electronic Transitions of Scandium Oxide

In addition to near-grazing reflection and transmission measurements of Sc0305 Diode, normal incidence transmission measurements were also taken from 2.9-3.5 nm. The positions of the L_2 and L_3 transitions are apparent when a graph of the transmittance is presented, as in Figure 44. In this figure, the drastic dips in the transmittance are due to photon absorption corresponding to the L_2 electronic transition at 3.069 nm (404.0 eV), and the L_3 electronic transition at 3.101 nm (399.9 eV). Comparison of these values for the positions of the peaks to those seen in a simulation of normal incidence transmission from the CXRO website shows a slight difference in transition position. In

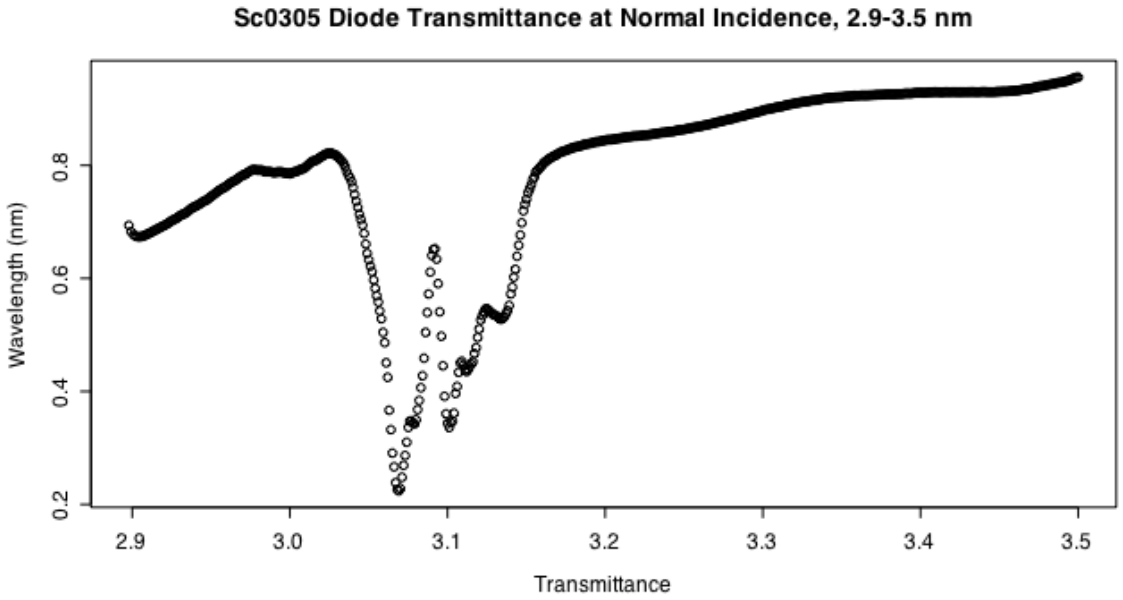

Figure 44: Measured transmittance (at normal incidence) of Sc0305 Diode from 2.9-3.5 nm shows noticeable dips at 3.069 and 3.101 nm (404.0 and 399.9 eV). These correspond to the L_2 and L_3 electronic transitions, respectively. Additional, smaller scale dips are also seen in the graph, at 3.079, 3.112, and 3.134 nm (402.7, 398.5, and 395.7 eV). These features are most likely due to the fine structure of Sc_2O_3.

the CXRO calculation of transmittance, the L_2 transition is seen at 3.056 nm (405.8 eV), and L_3 transition is evident at 3.090 nm (401.3 eV). These are seen in the transmittance graph shown in Figure 45.

The differences in the positions of the electronic transitions can be traced to the method used for calculating the optical constants of a compound. It is generally considered acceptable to calculate the optical constants of a compound in the EUV and x-ray region using the optical constants of the parent materials. The optical constants of the constituents of a compound are averaged together, weighted accordingly by their stoichiometric ratio. Though it is acknowledged that the bonding among the constituents of a compound will shift the positions of the electronic transitions, this is not taken into account when the optical constants of a compound are generated in this way. Therefore, the positions of the electronic transitions found in the CXRO database for scandium oxide are actually the electronic transition positions of scandium.

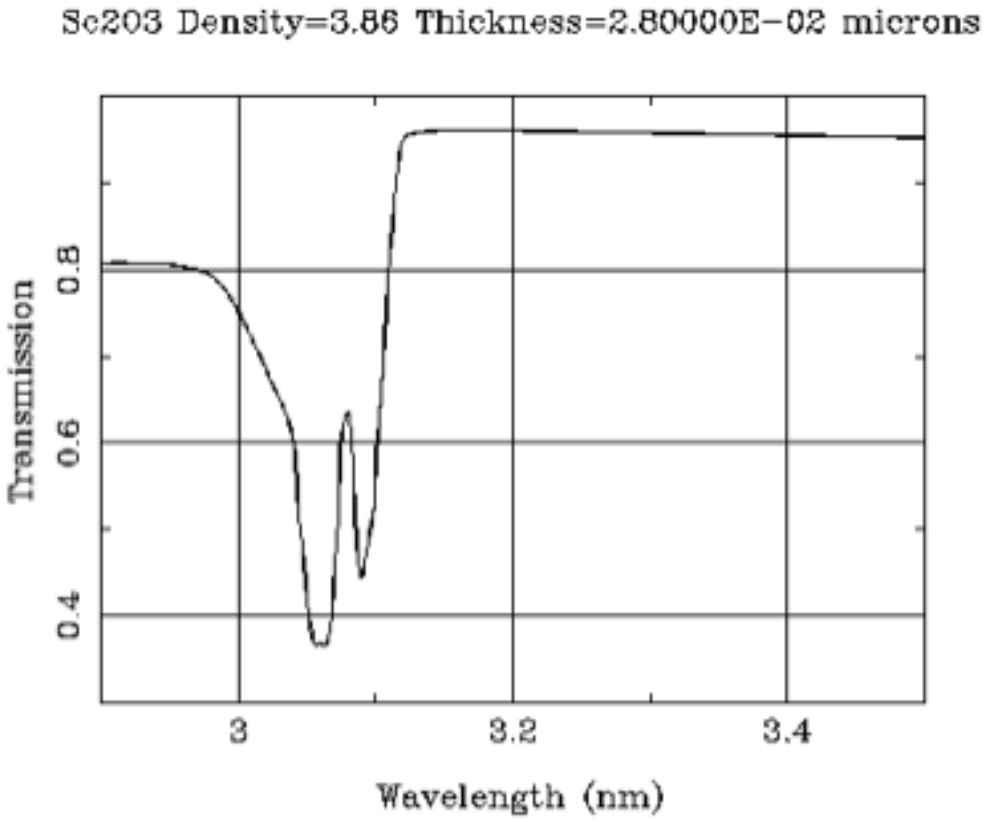

Figure 45: The calculated transmittance graph shows the locations of the L_2 and L_3 electronic transitions of scandium oxide available from the CXRO tables. The L_2 transition is seen at 3.056 nm (405.8 eV), and the L_3 transition appears at 3.090 nm (401.3 eV). These transition positions are actually those of scandium, since the computation does not shift the positions of the compound from that of its constituents.

There is also evidence of a shift in the position of the M electronic transition, at longer wavelengths. Figure 36 shows the measured optical constants of scandium oxide, as well as the values for n and k available from the CXRO website. The CXRO values show that scandium exhibits an electronic transition at 30 nm, or 41.3 eV (identified by the local maximum in the absorption coefficient, and the presence of a "dip-peak" feature in the index of refraction). Though the measured optical constants for scandium oxide, shown in Figure 39, only cover up to 30 nm, it is clear that the electronic transition is actually positioned at a longer wavelength. The trend established by the measured absorption coefficient k for scandium oxide in Figure 39 suggests the maximum is actually nearer 31.5 nm (39.4 eV). In the index of refraction curve, the "dip-peak" feature can also be used to determine the position of the transition, which occurs at the inflection point between the dip and the peak. Even though this inflection point is not present in the measured values, the position of the dip in the n values is easily seen. The CXRO values for n have the dip at 26.5 nm (46.8 eV), while the measured n has a dip at 28.5 nm (43.5 eV). This shift in the position of the "index-dip" to a longer wavelength suggests that the inflection point of n, and therefore the position of the electronic transition, is at a longer wavelength, as well. This supports the shift seen in the graph of the absorption coefficient. The shift of the electronic transition positions (both the L and M transitions) to longer wavelength (lower energy) is a surprising observation, as it is typical for such shifts due to oxidation to be in the opposite direction.

This observation of the shift in transition positions remains curious, given that the binding energies of scandium and scandium oxide are related in the usual fashion. The binding energy of the oxide is greater than that of the metal. For example, the binding energy of scandium $2p^{3/2}$ is 398.6 eV, while the binding energy of scandium oxide $2p^{3/2}$ is 403.2 eV.[32] The increase in the nuclear attraction binding the scandium valence electrons can be explained by these electrons being partially transferred to oxygen, which raises the total nuclear attraction. Though binding energy and photoabsorption are different properties, it is unexpected that they would have opposite trends. This behavior is an unexpected contrast, which warrants further study.

Figure 44 also shows smaller scale dips in the transmittance at 3.079, 3.112, and 3.134 nm (402.7, 398.5, and 395.7 eV). These are believed to be due to the fine structure of scandium oxide. Though these are intriguing features in the data, they were not explored further. The presence of these features, however, can be taken as a testament to the quality of the transmission data collected at normal, as well as resolution available from the instruments of Beamline 6.3.2 at the ALS.

9 Summary

9.1 Results

Simultaneous reflection and transmission measurements were made of a 28 nm thick scandium oxide thin film deposited on a silicon photodiode. Analysis of the reflection and transmission data collected produced the optical constants for scandium oxide. The values for the index of refraction n and the absorption coefficient k in the range from 4.5-30 nm are the results of simultaneous modeling of the reflection and transmission data using a matrix multiplication method for calculating reflectance and transmittance.

Scandium oxide thin films have been studied on a variety of substrates, including silicon wafers and silicon photodiodes. HRTEM, STEM, and EDX characterization of the coated photodiode from which measurements were made in the EUV showed this coating to be a bilayer. The bimodal property of the coating was included in the sample description during the EUV data analysis.

The method developed for collecting the data from the sample is a novel approach to studying thin films in the EUV. Most researchers studying thin films in the EUV make transmission measurements, either from free standing thin film samples or from coated photodiodes. These measurements are analyzed to find k, while n is found by applying a Kramers-Kronig analysis to the determined k. This experiment is the first to measure both reflection and transmission simultaneously. Additionally, the method for analyzing the data is unconventional, as both n and k are found in the analysis of the data. In this project, a set of variable-angle reflection and transmission data at a single wavelength is analyzed to produce values for both n and k directly from the measurements made of the thin film.

From the CXRO website, the L_2 transition of scandium is noted to be at 3.056 nm (405.8 eV), and the L_3 transition at 3.090 nm (401.3 eV). The measurements made of scandium oxide show the L_2 and L_3 transitions to be at 3.069 and 3.101 nm (404.0 and 399.9 eV), respectively. At the longer EUV wavelengths, scandium exhibits an M transition at 30.0 nm (41.3 eV). Measurements of scandium oxide in this area suggest that the transition occurs at a longer wavelength, approximately 31.5 nm (39.4 eV). Unfortunately, only a portion of this transition region is described by the results of this study. This trend for the electronic transition positions to shift to lower energies when scandium oxidizes is unexpected, and warrants further study. The optical properties of compound materials could perhaps be more accurately described if the shift in the position of the transitions is included in

the generation of optical constants for a compound from its constituents. Measurements of scandium oxide may contribute to the refinement of the method used for calculating n and k for a compound.

9.2 Conclusions

In addition to this project delivering the results described in the previous section, several conclusions can be drawn from the work completed along the way.

Through HRTEM, STEM, and EDX analysis, it was learned that the thin film of scandium oxide available was not a simple single layer coating. The sample chosen as the focus of the project, Sc0305, is actually a bilayer. Without examination by HRTEM and STEM, though, this sample would have most likely been mistakenly described as a monolayer in subsequent analysis. If the bimodal qualities of the sample had been overlooked, any results coming from analysis in which the film was incorrectly described would be in error, with the potential to mislead future work. It should become standard practice to verify the structure and quality of a film or family of films before detailed analysis of optical data is performed.

Continued use of the simultaneous reflection and transmission data collection technique will surely refine the process so that the issues found with the quality of the variable-angle transmission data (primarily at the shorter wavelengths) is resolved. The method of collecting data at a single θ over a range of wavelengths may be to blame for the anomalous features seen in the transmission measurements. By collecting the preferred data (a θ-2θ measurement at a single wavelength) directly, the quality of the transmission data may be found to improve. However, this will require more care to be taken during data collection, as different preamplifier gain settings will need to be used over different portions of the θ range, for both the reflection and transmission channels. Since gain changes cannot be made during the data collection sequence, several measurements at different gains may have to be collected, with the optimal parts of each collection selected for constructing a data file resembling the optical response of the coating from 10-80 degrees.

Though care was taken when data was collected in the shorter wavelength ranges, the data from 2.9-3.5 nm would have benefited from more closely spaced θ points. With measurements made every 0.2 or 0.25 degree, in contrast to every 0.5 degree, the resolution of the features of the interference pattern will improve. More data points in this region may also contribute to more robust analysis, and resolve the issue encountered with the divergence of modeled optical constants from the appropriate values.

Also in the 2.9-3.5 nm wavelength range, the reflection signal diminished rapidly with increasing incident angle. Typically, the signal had decreased to being under the noise floor by about 18 degrees. At the time Sc0305 was measured, it was not deemed worthwhile to continue collecting data to larger θ values. However, continuing data collection to 60 or even 80 degrees may prove advantageous. In doing so, the transmission data will benefit from more data points to define the plateau of the transmission curve, which will in turn allow for better analysis of the transmission data. Also, this will provide useful information about the dark current present in the reflection signal. The portion of the reflection measurement beyond about 18 degrees where the signal becomes buried in the noise can be used to establish a value for the dark current, which will be specific to the exact time of the data collection.

On the other end of the ALS EUV spectrum, the presence of higher-order harmonic light in the 25-50 nm wavelength range needs to be addressed. In principle this is most easily resolved by taking advantage of wavelength range overlap and comparing the amplitudes of reflectances at low angles (or transmittances amplitudes at high angles) measured in the 17.5-30 nm wavelength range to measurements taken in the 25-50 nm range. Adjustments can be made to the angular position of the three-bounce, order-suppressing mirror should be done until the reflectances in both wavelength ranges are brought into agreement. If a suitable angle cannot be found, a different coating for the mirrors or coatings of different materials will have to be chosen.

References

1. D. Attwood, *Soft X-rays and Extreme Ultraviolet Radiation: Principles and Applications,* (Cambridge University Press, Cambridge, 1999).

2. M. Ohring, *The Materials Science of Thin Films*, (Academic Press, San Diego, 1992).

3. W. R. Hunter, *App. Opt.* **21** (12) 2103 (1982).

4. O. S. Heavens, *Optical Properties of Thin Solid Films*, (Dover Publications, New York, 1965)

5. E. V. Kleber and B. Love, *The Technology of Scandium, Yttrium, And The Rare Earth Metals*, (Macmillan, New York, 1963).

6. Scandium Applications, Occurence, and Isoltation, http://en.wikipedia.org/wiki/Scandium.

7. I.V. Arkhangel'skii, L. N. Komissarova, G. Ya. Pushkina, E. G. Teterin, *Russ. J. of In. Chem.* **12** (7) 924.

8. J. H. Weaver and C. G. Olson, *Phys. Rev. B* **16** (2) 731 (1977).

9. Yu. A. Uspenskii, V.E. Levashov, A.V. Vinogradov, A. I. Fedorenko, V.V. Kondratenko, Yu. P. Pershin, E. N. Zubarev, and V. Yu. Fedotov, *Opt. Lett.* **23** 771 (1998).

10. J. F. Seely, Yu. A. Uspenskii, Yu. P. Pershin, V. V. Kondratenko, and A. V. Vinogradov, *App. Opt.* **41** (10) 1846 (2002).

11. D. L. Windt, S. M. Kand and G. E. Sommargren, *Proc. SPIE* **4851**, 441 (2002).

12. J. Arthur and R. Tatchyn, *Proc. SPIE* **4143**, 1 (2001).

13. S. S. Andreev, H. -Ch. Mertins, Yu. Ya Palonov, N. N. Salsshchenko, Fl Schaters, E. A. Shamov, and L. A. Snmaenok, *Nucl. Instrum. Methods Phys. Res. A* **448**, 113 (2000).

14. F. Schafers, *Physica B* **283**, 119 (2000).

15. F. Eriksson, G. A. Johansson, H. M. Hertz, E. Gullikson, U. Kreissig, J. Birch, *Opt. Lett.* **28** (24) 2494 (2003).

16. Yu. A. Uspenskii, J. F. Seely, N. L. Popov, A. V. Vinogradov, Yu. P. Pershin, and V. V. Kondratenko, *J. of Opt. Soc. of Am. A* **21** (2) 298 (2004).

17. J. I. Larruquert, J. A. Aznarez, J. A. Mendez, A. M. Malvezzi, L. Pletto, and S. Covini, *App. Opt.* **43** (16) 3271 (2004).

18. J. F. Seely, *App. Opt.*, **41** (28) 5979 (2002).

19. A. L. Aquila, F. Salmassi, E. M Gullikson, F. Eriksson, and J. Birch, *University of California eScholarship Repository*, LBNL-58403.

20. First Reaction Product Spec Sheet for 4" Scandium Sputter Target; First Reaction, 37 Depot Road, Hampton Falls, New Hampshire 03844.

21. G. Acosta, D. D. Allred, and R. C. Davis, *Soc. of Vac. Coaters 2005 48th Ann. Tech. Con. Proc.,* **48** (1) 707 (2005).

22. E. M. Gullikson, R. Korde, L.R. Canfield, R. E. Vest, *J. of Elec. Spec. and Related Phenomena* **80** 313 (1996).

23. D. D. Allred, G. A. Acosta, N. F. Brimhall, and R. S. Turley, *Soc. of Vac. Coaters 2006 49th Ann. Tech. Con. Proc.*, **49** (1) 314 (2006).

24. A. R. Kortan, N. Kopylov, J. Kwo, M. Hong, C. P. Chen, J. P. Mannaerts, and S. H. Liou, *Appl. Phys. Lett.* **88** 021906 (2006).

25. Advanced Light Source High-Resolution EUV Calibration and Standards Beamline 6.3.2, http:/als.lbl.gov/als/als_users_bl/6.3.2-Datasheet.pdf.

26. S. Turley, *Validation of Optics Codes*, Brigham Young University Department of Physics Topic Notes (2006).

27. M. Sigirst, G. Chassaing, J. C. Francios, F. Antonageli, N. Zuma, and M. Piacentini, *Phys. Rev. B* **35** (8) 3760 (1987).

28. A. Caticha, *Phys. Rev. B* **52** (13) 9214 (1995).

29. D. K. G. de Boer, *Phys. Rev. B* **49** (9) 5817 (1994).

30. R. Swanepoel, *J. of Phys. E: Sc. Instr.* **16** 1214 (1983).

31. B. P. Gila, J. W. Johnson, R. Mehandru, B. Luo, A.H. Onstine, K. K. Allums, V. Krishnamoorthy, S. Bates, C.R. Abernathy, F. Ren, and S. J. Pearton, *Phys. Stat. Sol.* **188** (1) 239 (2001).

32. J. K. Gimzewski, D. J, Fabian, L. M. Watson and S. Affrossman, *J. Phys. F: Metal Physics* **7** (11) L305 (1977).